AGU PUBLICATIONS

JGR

Journal of Geophysical Research: Solid Earth

RESEARCH ARTICLE
10.1002/2017JB014230

Key Points:
- A new centroid moment tensor catalogue based on a 3-D Earth model for the region of north of Australia has been constructed
- A significant effect of 3-D heterogeneity in source parameter inversions has been documented
- Newly obtained earthquake locations provide new tectonic constraints on the Papua New Guinea and Solomon Islands

Correspondence to:
B. Hejrani,
babak.hejrani@anu.edu.au

Citation:
Hejrani, B., H. Tkalčić, and A. Fichtner (2017), Centroid moment tensor catalogue using a 3-D continental scale Earth model: Application to earthquakes in Papua New Guinea and the Solomon Islands, *J. Geophys. Res. Solid Earth*, *122*, 5517–5543, doi:10.1002/2017JB014230.

Received 21 MAR 2017
Accepted 10 JUL 2017
Accepted article online 12 JUL 2017
Published online 30 JUL 2017

Centroid moment tensor catalogue using a 3-D continental scale Earth model: Application to earthquakes in Papua New Guinea and the Solomon Islands

Babak Hejrani[1], Hrvoje Tkalčić[1], and Andreas Fichtner[2]

[1]Research School of Earth Sciences, Australian National University, Canberra, ACT, Australia, [2]Department of Earth Sciences, ETH Zurich, Zurich, Switzerland

Abstract Although both earthquake mechanism and 3-D Earth structure contribute to the seismic wavefield, the latter is usually assumed to be layered in source studies, which may limit the quality of the source estimate. To overcome this limitation, we implement a method that takes advantage of a 3-D heterogeneous Earth model, recently developed for the Australasian region. We calculate centroid moment tensors (CMTs) for earthquakes in Papua New Guinea (PNG) and the Solomon Islands. Our method is based on a library of Green's functions for each source-station pair for selected Geoscience Australia and Global Seismic Network stations in the region, and distributed on a 3-D grid covering the seismicity down to 50 km depth. For the calculation of Green's functions, we utilize a spectral-element method for the solution of the seismic wave equation. Seismic moment tensors were calculated using least squares inversion, and the 3-D location of the centroid is found by grid search. Through several synthetic tests, we confirm a trade-off between the location and the correct input moment tensor components when using a 1-D Earth model to invert synthetics produced in a 3-D heterogeneous Earth. Our CMT catalogue for PNG in comparison to the global CMT shows a meaningful increase in the double-couple percentage (up to 70%). Another significant difference that we observe is in the mechanism of events with depth shallower then 15 km and $M_w < 6$, which contributes to accurate tectonic interpretation of the region.

1. Introduction

1.1. Seismic Moment Tensor Inversion

The accurate estimation of earthquake source parameters and 3-D Earth structure is one of the main goals in seismology. The global centroid moment tensor (GCMT) algorithm [*Dziewonski et al*., 1981] has been routinely applied to seismic data for 35 years. The catalogue has been quite successful. *Hjörleifsdóttir and Ekström* [2010] studied the effect of 3-D Earth structure on the GCMT catalogue and found tens of kilometers difference in lateral location and depth. They also observed that the variations in moment tensor components depend on the 3-D structure. Improving our knowledge about the 3-D structure of the Earth results in a more accurate estimation of its impulse response or Green's function, which consequently results in a better estimation of the mechanism acting in the source region. Significant effort in recent decades has gone into improving and developing methods to calculate the wavefield propagation through the Earth. Advances in numerical wave propagation and the increasing computational resources now allow us to compute the complete wavefield through 3-D media with high accuracy [e.g., *Komatitsch and Tromp*, 1999; *Fichtner et al*., 2009a].

Significant cost and time is required for the simulation of wave propagation through a 3-D heterogeneous medium, which makes it difficult to investigate the effect of 3-D heterogeneity in studies of the seismic source. Most source studies use a spherically symmetric Earth model to calculate Green's functions needed to estimate the independent elements of the moment tensor (MT) [*Kikuchi and Kanamori*, 1991; *Zahradnik et al*., 2005]. A search for the optimum 3-D point source location of the centroid usually follows. It has been shown that using stations at local distances, 1-D layered crustal structure can provide a reasonable fit to the data filtered at around 20–50 s and even down to 10 s under specific circumstances [*Zahradnik et al*., 2005; *Adamová et al*., 2009]. However, in an environment with significant lateral velocity variations, e.g., around an active volcano, the 1-D Earth model by definition ignores the lateral heterogeneity and therefore produces incomplete/erroneous Green's functions which will result in incorrect estimation of source parameters. Researchers have tried using several 1-D velocity models (a velocity

model per each source station) to partially account for lateral velocity variations [e.g., *Dreger et al*., 2000; *Tkalčić et al*., 2009].

With significant advancements in computational power during the past decades, the numerical calculation of the wavefield through a 3-D anisotropic, heterogeneous medium has become feasible. There have been several studies addressing this issue and all have general consensus that the use of 3-D heterogeneous Earth models improves source parameter retrieval [e.g., *Gallovič et al*., 2010; *Fichtner and Tkalčić*, 2010; *Kim et al*., 2011; *Hingee et al*., 2012; *Kühn and Vavryčuk*, 2013].

Assuming that the location of the earthquake is known, the number of simulations required to perform an MT inversion is proportional to the number of the events. However, in the CMT approach [*Dziewonski et al*., 1981], the centroid location and time are searched simultaneously with the six independent components of the MT. A common way is to perform a grid search on a predefined grid around the source region [*Serpetsidaki et al*., 2010; *Sokos et al*., 2012]. Considering the size of our study area, this would require a large and impractical calculation of Green's functions. Considering this time and cost, we use the reciprocity theorem to calculate the Green's functions.

The source-receiver reciprocity has been well known and used in exploration seismology [e.g., *Claerbout*, 1976; *Chapman*, 1994; *Červený*, 2001], remote sensing [*de Hoop and de Hoop*, 2000], and waveform modeling [*Bouchon*, 1976; *Graves and Clayton*, 1992; *Graves and Wald*, 2001]. Recently, the application of reciprocity to source studies attracted much attention, mainly on local and regional scales, i.e., for source-receiver distances less than 1000 km [*Okamoto*, 2002; *Süss and Shaw*, 2003; *Lee et al*., 2011; *Zhu and Zhou*, 2016]. In this study, the reciprocity theorem has been used to reduce the number of calculations to an extent where the wavefield on tens of thousands of grid points can be calculated in a significantly shorter time frame.

Eisner and Clayton [2001, 2005] used a finite difference method to calculate reciprocal Green's functions to build 300 source scenarios for five major Southern California faults in the 3-D heterogeneous crustal model of *Magistrale et al.* [2000]. *Liu et al.* [2004] used a spectral-element method to calculate strain Green's tensors for CMT inversion in a 3-D crustal model of Southern California [*Süss and Shaw*, 2003]. *Lee et al.* [2011] followed the same approach and developed an automated procedure to obtain CMT solutions. *Zhu and Zhou* [2016] applied the same method to calculate CMT solutions of the 2013 Lushan earthquake and its aftershocks. In all these publications a meaningful improvement in waveform fit has been observed.

Hingee et al. [2012] initiated a preliminary study to adapt the CMT solution to continental scales using a 3-D heterogeneous velocity model of the Australasian region called AMSAN19 [*Fichtner et al*., 2009b; *Fichtner et al*., 2010]. However, they did not invert for the centroid location, depth, and time. We peruse this study further by using a spectral-element method to compute a library of Green's functions on a 3-D grid covering Papua New Guinea, the Bismarck Sea, and the Solomon Islands. We then use this library to calculate CMT solutions for earthquakes that occurred with $M_w > 5.0$ from 2006 to 2016 in this region.

1.2. Tectonic Settings

The tectonic regime of the study area is complex (Figure 1a). This is where two of the Earth's major lithospheric plates interact: the Australian and the Pacific plates [e.g., *Hill and Hall*, 2003].

The Australian continent is moving north-east and colliding with the Pacific plate at a rate of ~110 mm per year [*Johnson and Molnar*, 1972; *Davies et al*., 1987]. The convergence creates one of the most seismically active regions on Earth, with earthquakes of magnitude up to 8.0. A number of smaller plates form a complicated tectonic setting which compensates the collision between the two major plates [*Tregoning et al*., 1998; *Wallace et al*., 2004].

Toward the north, the main compensation occurs along the Bismarck Sea Seismic Lineation (BSSL) where the North Bismarck plate slides toward the west relative to the South Bismarck plate [*Tregoning et al*., 1998; *Llanes et al*., 2009; *Koulali et al*., 2015]. Further north-east, the most recent GPS data analysis [*Koulali et al*., 2015] showed an oblique convergence of ~93 mm per year across the New Guinea Trench (Figure 1a).

The South Bismarck Sea plate collides with the Solomon Sea plate at its southern edge, where the megathrust New Guinea Trench is located. The subduction of the Solomon Sea plate continues toward west, south-west beneath the Pacific plate [*Tregoning et al*., 1998].

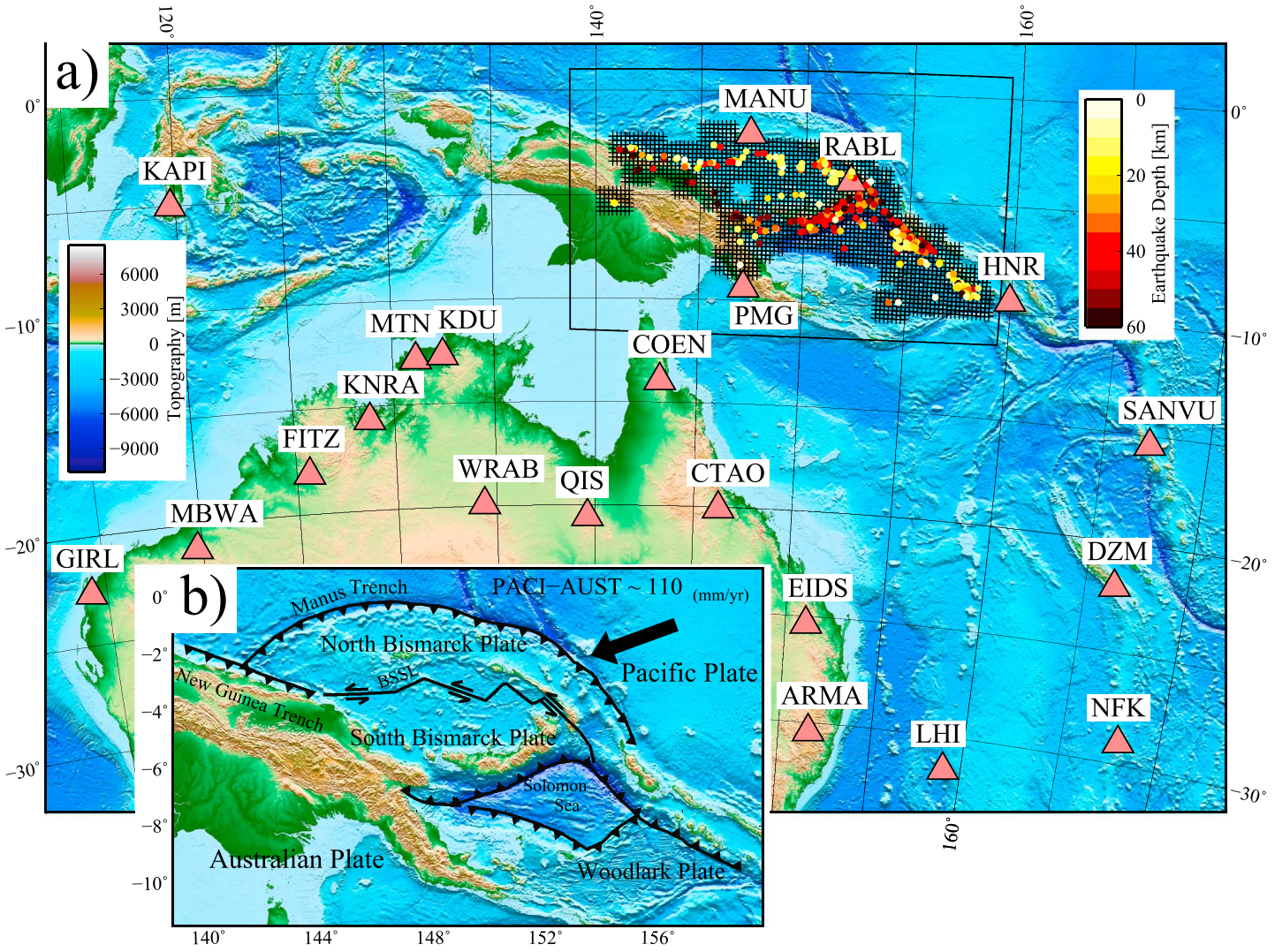

Figure 1. (a) Map of the topography, seismic stations, 318 events used in this study, and grid points used for the calculation of synthetic Green's functions using the reciprocity principle. (b) Map view of tectonic setting in Papua New Guinea region.

Such a complex and highly active tectonic environment acts as a seismological laboratory to investigate the effect of 3-D Earth heterogeneity on earthquake source parameters. We selected events with depth <50 km (quasi-crustal events) that occurred during 10 years (2006–2016) within the mentioned tectonic boundaries (Figure 1).

2. Methodology and Data Processing

2.1. Method

A seismic source generates waves that travel through the Earth and are recorded at seismic stations. Seismic waves carry information from the source and the Earth structure along their wave path. Separating the source effect from the structure effect, the displacement at location x due to an impulsive force at location x_0 can be defined as follows [*Shearer*, 1999]:

$$U_i(x) = G_{ij}(x;x_0)^* f_j, \tag{1}$$

where U_i is the displacement in the $\hat{i}$ direction ($\hat{i}$ is a unit vector), f_j is a pulse force along $\hat{j}$, G_{ij} is the elastodynamic Green's function from x_0 to x, and * represents the convolution over time. Equation (1) can explain the

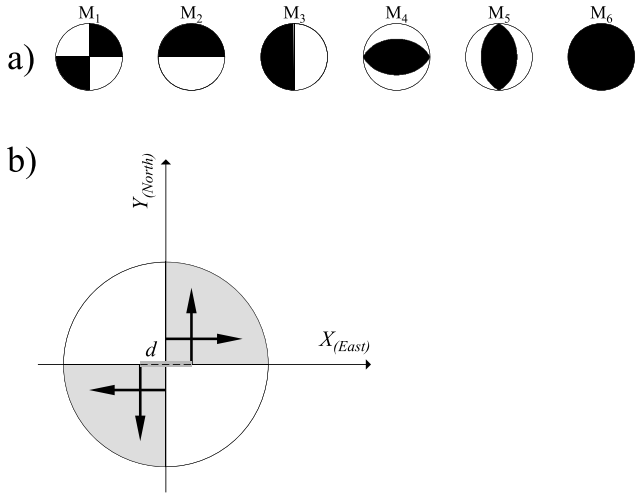

Figure 2. (a) Six elementary basis mechanisms in equation (5). (b) Plot of forces for the first elementary basis M_1. The offset d in equations (6) and (13) is the distance between the center of the beach ball and each force.

displacement resulting from any combination of forces. For example, the displacement due to a couple acting at x_0 [*Burridge and Knopoff*, 1964] can be written as

$$U_i(x) = \lim_{d\to 0} \frac{G_{ij}\left(x; x_0 + \hat{k}d\right) * f_j - G_{ij}\left(x; x_0 - \hat{k}d\right) * f_j}{2d} = \frac{\partial G_{ij}(x; x_0)}{\partial (x_0)_{\hat{k}}} * f_j(2d), \tag{2}$$

where the forces f_j are separated by the distance $2d$ in the $\hat{k}$ direction. The product $f_j(2d)$ can be generalized for the point source approximation of the seismic source moment tensor [*Backus and Mulcahy*, 1976]:

$$U_i(x) = \frac{\partial G_{ij}(x; x_0)}{\partial (x_0)_{\hat{k}}} * M_{jk}, \tag{3}$$

where M_{jk} represents a couple of opposite forces along $\hat{j}$ with infinitesimal separation in the $\hat{k}$ direction. The general moment tensor M can be represented as a linear combination of a set of elementary MTs, M_m [*Kikuchi and Kanamori*, 1991; *Zahradnik et al.*, 2005; *Mustać and Tkalčić*, 2016]:

$$M = \sum_m M_m a_m, \tag{4}$$

where a_m are the coefficients. In this study we adopted the convention in which six elementary MTs are defined as (Figure 2a):

$$\begin{aligned} M_1 &= \begin{bmatrix} 0 & 1 & 0 \\ 1 & 0 & 0 \\ 0 & 0 & 0 \end{bmatrix}; \; M_2 = \begin{bmatrix} 0 & 0 & 1 \\ 0 & 0 & 0 \\ 1 & 0 & 0 \end{bmatrix}; \; M_3 = \begin{bmatrix} 0 & 0 & 0 \\ 0 & 0 & -1 \\ 0 & -1 & 0 \end{bmatrix} \\ M_4 &= \begin{bmatrix} -1 & 0 & 0 \\ 0 & 0 & 0 \\ 0 & 0 & 1 \end{bmatrix}; \; M_5 \begin{bmatrix} 0 & 0 & 0 \\ 0 & -1 & 0 \\ 0 & 0 & 1 \end{bmatrix}; \; M_6 = \begin{bmatrix} 1 & 0 & 0 \\ 0 & 1 & 0 \\ 0 & 0 & 1 \end{bmatrix} \end{aligned} \tag{5}$$

in the Cartesian coordinates corresponding to north, east, and up. The advantage of using this convention is that certain solutions, such as pure deviatoric or pure double couple, can be obtained through different subgroups of the six elementary MTs. For example, pure deviatoric is represented by M_1–M_5. Ground

motion on the vertical component at location x due to M_1 located at location x_0, in terms of equations (2) and (3), can be expressed as

$$E_z(x) = \lim_{d\to 0}\frac{G_{zn}(x;x_0+\hat{e}d)f_n - G_{zn}(x;x-\hat{e})f_n}{2d} + \lim_{d\to 0}\frac{G_{ze}(x;x_0+\hat{n}d)f_e - G_{ze}(x;x_0-\hat{n}d)f_e}{2d}$$
$$= \frac{\partial G_{zn}(x;x_0)}{\partial(x_0)_{\hat{e}}}M_{ne} + \frac{\partial G_{ze}(x;x_0)}{\partial(x_0)\hat{n}}M_{en}, \tag{6}$$

where $\hat{n}$ and $\hat{e}$ are the unit vectors along north and east, respectively; E_z is the elementary seismogram recorded on the vertical component; and f_n and f_e are the forces along north and east, but separated along the perpendicular direction (Figure 2b). The reciprocal version of equation (6), to be discussed in detail in section 3.1, is used to produce synthetic seismograms in this study.By substituting the equivalent linear combination for M from equation (4) into equation (3), a seismogram can be expressed as a linear combination of six elementary seismograms:

$$U_i(x) = \sum_{m=1}^{6}\left(\frac{\partial G_{ij}(x;x_0)}{\partial(x_0)_{\hat{k}}} * M_m\right)a_m. \tag{7}$$

Equation (7) can be written in a more simplified matrix form for real data:

$$\boldsymbol{U} = E\boldsymbol{A}, \tag{8}$$

where $\boldsymbol{U}$ is the vector of observed data (displacement amplitudes from three-component seismic stations), $\boldsymbol{A}$ is the vector of six MT coefficients to be determined, and E is the matrix of elementary seismograms (with size of 6 by length of U). We use the least squares method to estimate the vector of the coefficients, $\boldsymbol{A}$:

$$\left(E^T E\right)^{-1}\left(E^T\boldsymbol{U}\right) = \boldsymbol{A_{est}}. \tag{9}$$

where $\boldsymbol{A_{est}}$ is our estimation vector of coefficients $\boldsymbol{A}$. The six independent components of the moment tensor can then be calculated from the estimated a_i coefficients:

$$M_{est} = \begin{bmatrix} -a_4+a_6 & a_1 & a_2 \\ a_1 & -a_5+a_6 & -a_3 \\ a_2 & -a_3 & a_4+a_5+a_6 \end{bmatrix}. \tag{10}$$

We assume that the earthquakes in this study are of a tectonic origin; thus, we leave out the volume component M_6 and calculate the deviatoric moment tensor, represented by the first five bases M_1 to M_5. For this, the coefficient a_6 is set to zero and the inversion only estimates the first five coefficients. Prior to the inversion, we compute a library of elementary seismograms on a 3-D grid, with horizontal spacing of 0.2 by 0.2° and vertical spacing of 4 km, covering the study area down to 70 km depth (dashed area in Figure 1a).The location and the time of the centroid of each earthquake are determined through a grid search as follows. For each earthquake, we run a grid search by repeating equation (9) over a selected set of nodes in the vicinity of a reference location (GCMT centroid) and a set of time shifts around the origin time (International Seismological Centre (ISC) report). The grid node and time shift that provide the highest variance reduction between the synthetics and the real data is defined as our CMT. The variance reduction was calculated using the following formula:

$$V.R. = 1 - \sqrt{\frac{\sum_{i=1}^{n}\left(U(i)-S(i)\right)^2}{\sum_{i=1}^{n}U(i)^2}}, \tag{11}$$

where U is the observed displacement, S is the synthetics, and i is the time index of each sample. The most crucial step in determining our CMT solutions is the preparation of "a library" of synthetic seismograms. We used the reciprocity theorem to precompute this library.

2.2. Numerical Simulations and Reciprocity Property of the Wavefield

The spectral-element code SES3D [*Fichtner et al*., 2009a] was used to calculate the synthetic waveforms. For the simulation of seismic wave propagation we used the networked Beowulf cluster Terrawulf (http://rses.anu.edu.au/TerraWulf/) and the large-scale peak system, Raijin, maintained by the Australian National Computational Infrastructure facility (NCI; http://nci.org.au/). Using 200 cores on Terrawulf II, it takes about 3 h to simulate the wavefield for one basis MT from a grid point to a station. The 3-D grid deployed in this study to account for all earthquakes of interest consists of 34,136 points which would require more than 200,000 calculations, hence impossible to implement.

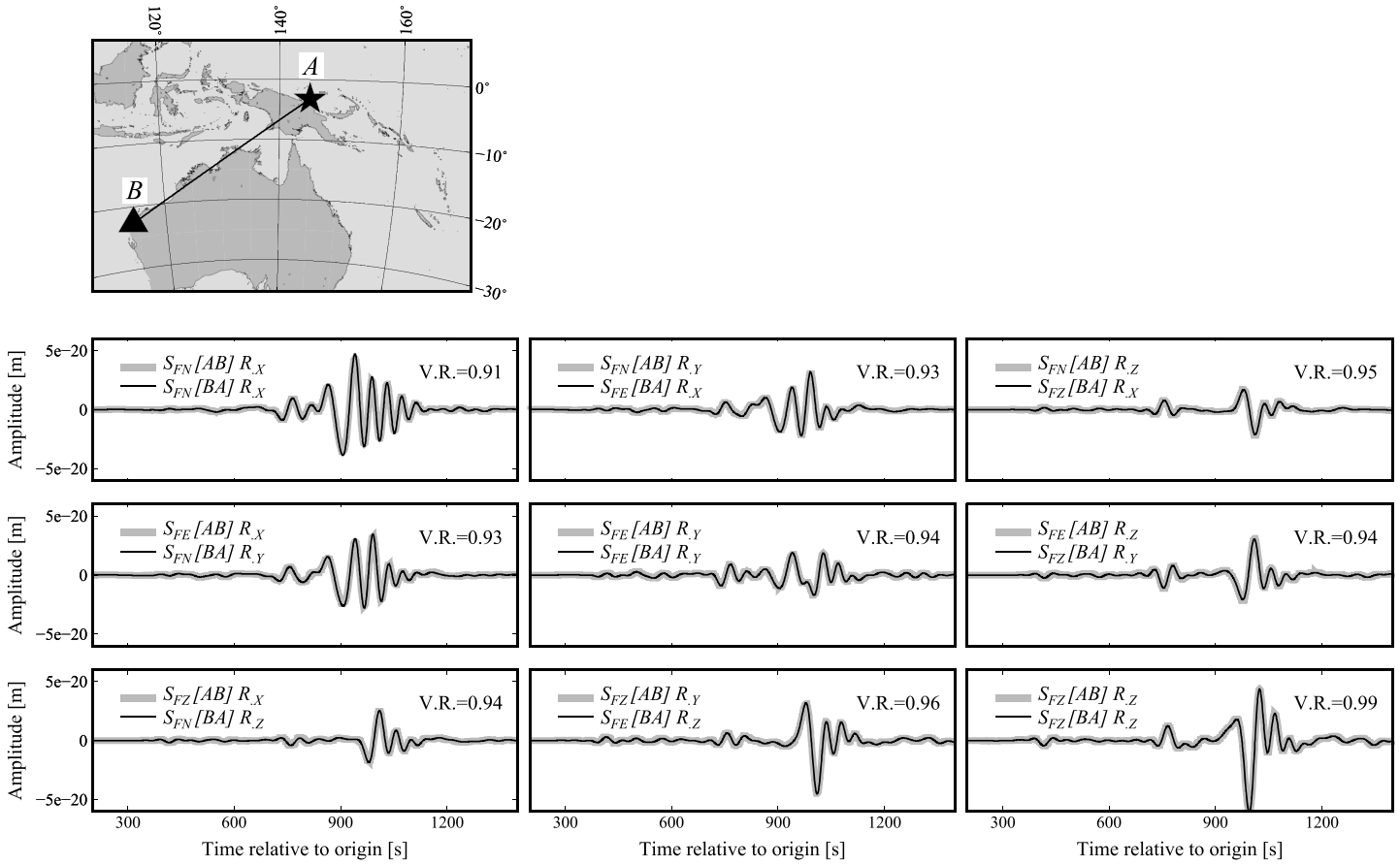

Figure 3. Nine pairs of Green's functions and their reciprocals for points A and B. These nine pairs account for all possible combination of the direction of the force and recording components. S_{FN}, S_{FE}, and S_{FZ} indicate forces pointing toward north, east, and up. $R_{.N}$, $R_{.E}$, and $R_{.Z}$ are seismic recorders along north, east, and up. The thick gray line represents the calculation of the wavefield from source A to receiver B, i.e., the direct calculation of the wavefield. The thin black line shows the reciprocal calculation of the wavefield from the source B to receiver A. The variance reductions between the direct and the reciprocal solutions are shown in the top right corner of each pair of waveforms.

Using the reciprocity theorem [*Eisner and Clayton*, 2001] we can efficiently calculate the wavefield between the source and the receiver by calculating the Green's functions from a single receiver to all grid nodes. This way the number of calculations will be proportional to the number of utilized stations. An implementation of the reciprocal property of the wavefield has been used both in waveform tomography [e.g., *Zhao et al.*, 2005; *Chen et al.*, 2007] and source parameter inversion [e.g., *Eisner and Clayton*, 2005; *Zhao et al.*, 2006; *Lee et al.*, 2011]. To test the accuracy of our numerical simulations, we compared nine possible pairs of direct and reciprocal Green's functions (three forces recorded in three orthogonal directions). Seismograms due to three forces pointing north, east, and up at location A in Figure 3, recorded on three-component seismometers located at B which is our station GIRL, versus their reciprocals show a variance reduction of 94–99%. Inaccuracies up to 6% could be due to numerical noise or reflections from different imperfect absorbing boundaries (absorbing boundaries are different for the direct and reciprocal propagations). The term G_{ij} in equation (1) could be replaced by its reciprocal pair, $\overline{G_{ji}}$:

$$G_{ij}(x;x_0)*f_j = \overline{G_{ji}}\ (x_0;x)*f_i, \tag{12}$$

and consequently, we can rewrite the synthetic seismogram expressed in equation (6) using reciprocal Green's functions of equation (12) [*Eisner and Clayton*, 2001]:

$$U_z(x) = \lim_{d\to 0}\frac{\overline{G_{nz}}(x_0+\hat{e}d;x)\ f_z - \overline{G_{nz}}(x_0-\hat{e}d;x)\ f_z}{2d} + \lim_{d\to 0}\frac{\overline{G_{ez}}(x_0+\hat{n}d;x)\ f_z - \overline{G_{ez}}(x_0-\hat{n}d;x)\ f_z}{2d}, \tag{13}$$

and the same reciprocity properties can be applied to the other five MT bases, M_2 through M_6. We place three

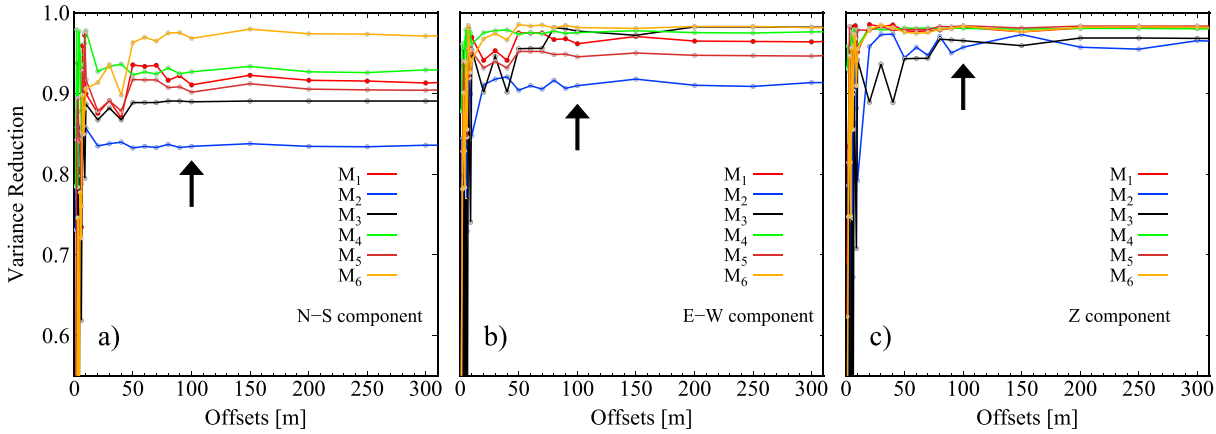

Figure 4. Variance reduction between the direct and reciprocal seismograms for all six elementary bases is plotted against half of the offset (distance between the force and the grid node in the center), *d*, in equations (6) and (13). This is shown for (a) north-south, (b) east-west, and (c) vertical components. The black arrow marks the distance we chose in this study.

orthogonal forces at each station's location and calculate the wave propagation to all grid points. Then we record the displacement at a small offset to the target grid point. This provides reciprocal seismograms to calculate the first-order numerical spatial derivatives of the displacement for any grid point (note that equation (13) accounts only for M_1). This approach reduces the computational time to the time it takes run to one simulation multiplied by the factor of 3 to account for all stations and components.

In an analytical solution of equation (2) the derivative with respect to *d* is calculated. However, we face limitations when solving an equation numerically. We ran a test to build the six basic mechanisms following equation (5), using a range of offsets (from 10 to 950 m) and calculated the variance reduction between direct and reciprocal waveforms for each offset value (marked with *d* in Figure 2b). For offsets $>$100 m there is sufficient difference in the individual Green's functions that the numerical differentiation is stable and the variance reduction remains stable and above 90% (Figure 4). For the source and receiver specification in Figures 3 and 4 the plot of direct and reciprocal solutions of six elementary mechanisms where the offset is set to 100 meters shows reasonable agreement (Figure 5).

After setting the offset *d* in equation (6) to 100 m from each grid point, we generated waves for three forces pointing north, east, and vertical (up) from each station in Figure 1 (total of 21) to 34,136 grid points (dashed area in Figure 1b). For our 3-D model, AMSAN19, the total CPU hours, considering the memory limitations on Terrawulf and NCI clusters, was ~7500. For synthetic tests and comparisons between 1-D and 3-D models we calculated the reciprocal synthetics using the spherically symmetric ak135 [*Kennett et al.*, 1995] as well. These

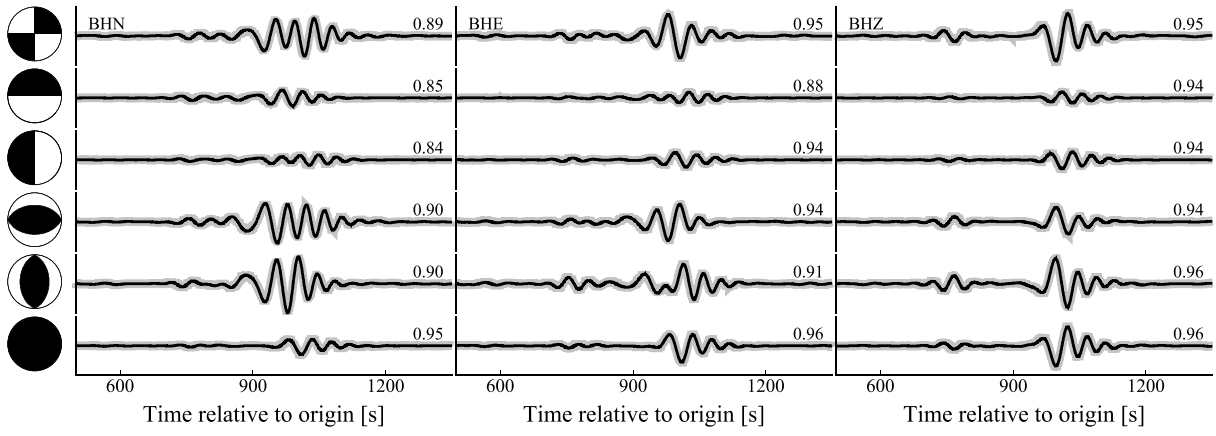

Figure 5. Reconstruction of ground motion for the six elementary seismograms for a source located at A and a receiver at B (see Figure 3 for the locations of A and B). Thick gray waveforms are calculated from source A to receiver B, and the thinner black line is made from reciprocal Green's functions as described in the text.

1-D and 3-D synthetic waveforms were used to carry out waveform inversion with both the observed and the synthesized data from designed scenarios discussed in the following sections.

For each CMT solution we selected stations from distances of 2°–45°. We compare our solutions, henceforth referred to as continental-scale CMT (CSCMT) to the global CMT (GCMT). CSCMTs calculated using AMSAN19 (3-D model) and ak135 (1-D model) are referred to as CSCMT-3D and CSCMT-1D, respectively. In this study, for comparing two MTs (for example, CSCMT-3D and GCMT solutions), we used the definition described in *Frohlich and Davis* [1999], who suggested that a 3 × 3 MT could be considered as a vector in a nine-dimensional space. Consequently, the difference between the two MTs can be seen as the angle between two vectors (in a nine-dimensional space), hereafter called ω_{9D}. For two pure DC MTs, ω_{9D} becomes zero if the mechanisms are identical and 180° if they have opposite *P* and *T* axes (e.g., reverse versus normal).

2.3. Data Processing

Raw data were corrected for instrument response, filtered using a Butterworth filter at 40–200 s period and resampled to 2 samples per second. The same filtering and resampling was applied to the synthetic seismograms. Since AMSAN19 predicts the complete waveform with reasonable accuracy at 40–200 s [*Fichtner et al*., 2009b, 2010], we did not limit the inversion to any specific window or wave type (*P*, *S*, or surface waves), and a full waveform (total length of 1400 s) was used in the inversion. Prior to the inversion, the quality of data was checked manually and the noisy stations or components were removed to avoid any bias from fitting the noise rather than actual signals.

3. Synthetic Tests

The goal of this section is to document the effect of using a 1-D layered Earth model (ak135 [*Kennett et al*., 1995]) on the CMT solution. For this, we present three synthetic tests where we invert synthetic data produced using the AMSAN19 model. The first five elementary mechanisms (Figure 2a) were used to produce the synthetics. We also document the error that is introduced by the reciprocal waveforms.

3.1. Case 1: Inversion for MT for Fixed Location and Time (Figure 6)

Data for five basis mechanisms M_1–M_5 (Figure 6a) from a source located in the Bismarck Sea at 7 km depth (yellow star on the map in Figure 6b) to 21 stations using AMSAN19 were simulated. In the first test, we fixed the lateral location, depth, and time of the centroid to the correct value and inverted only for five independent components of the MT (deviatoric MT inversion) using both AMSAN19 and ak135. The results show up to 40% drop in DC (Figure 6b) as well as ~80% drop in variance reduction when we use ak135 as Earth model. For example, the mechanism gets distorted from strike slip toward dip slip for the first basis MT. Since this test was performed without adding noise, the differences between the inputs and the outputs are the result of heterogeneities in the 3-D model. Using reciprocal Green's functions computed for AMSAN19, we obtain similar mechanisms to the inputs, as expected. The recovered mechanisms show up to 3% non-DC component with the fault strike, dip, and rake deviating only up to 1° from the true value. These small differences are due to numerical noise and inaccuracies of reciprocal Green's functions (discussed in section 2.2 and Figures 3 and 4). The effect of station coverage as well as using only distant stations that are more affected by the 3-D heterogeneities is tested by choosing different subsets of stations (Figures 6c and 6d). Using only eight stations at distances larger than 24° (with poor azimuthal coverage) and AMSAN19 as Earth model, we observed up to 9% drop in DC percentage of MT as well as up to 3° difference in fault plane strike, dip, and rake, while the variance reduction remains almost the same as that for the full station coverage in Figure 6b. The recovered mechanism using ak135 is erroneous and the total variance reduction drops to below zero (Figures 6c and 6d). The wavefield gets more distorted for longer paths through the 3-D heterogeneous structure (far stations). This plays an important role in progressively worsening the results, which is seen in Figures 6b–6d. The erroneous mechanisms here partially account for the distortion caused by the 3-D heterogeneity.

3.2. Case 2: Inversion for MT and Time for a Fixed Location (Figure 7)

In this test, we repeated the previous case including a grid search around the correct reference time. In the presence of good azimuthal coverage (Figure 7b) using ak135, the DC percentage increases (except for the

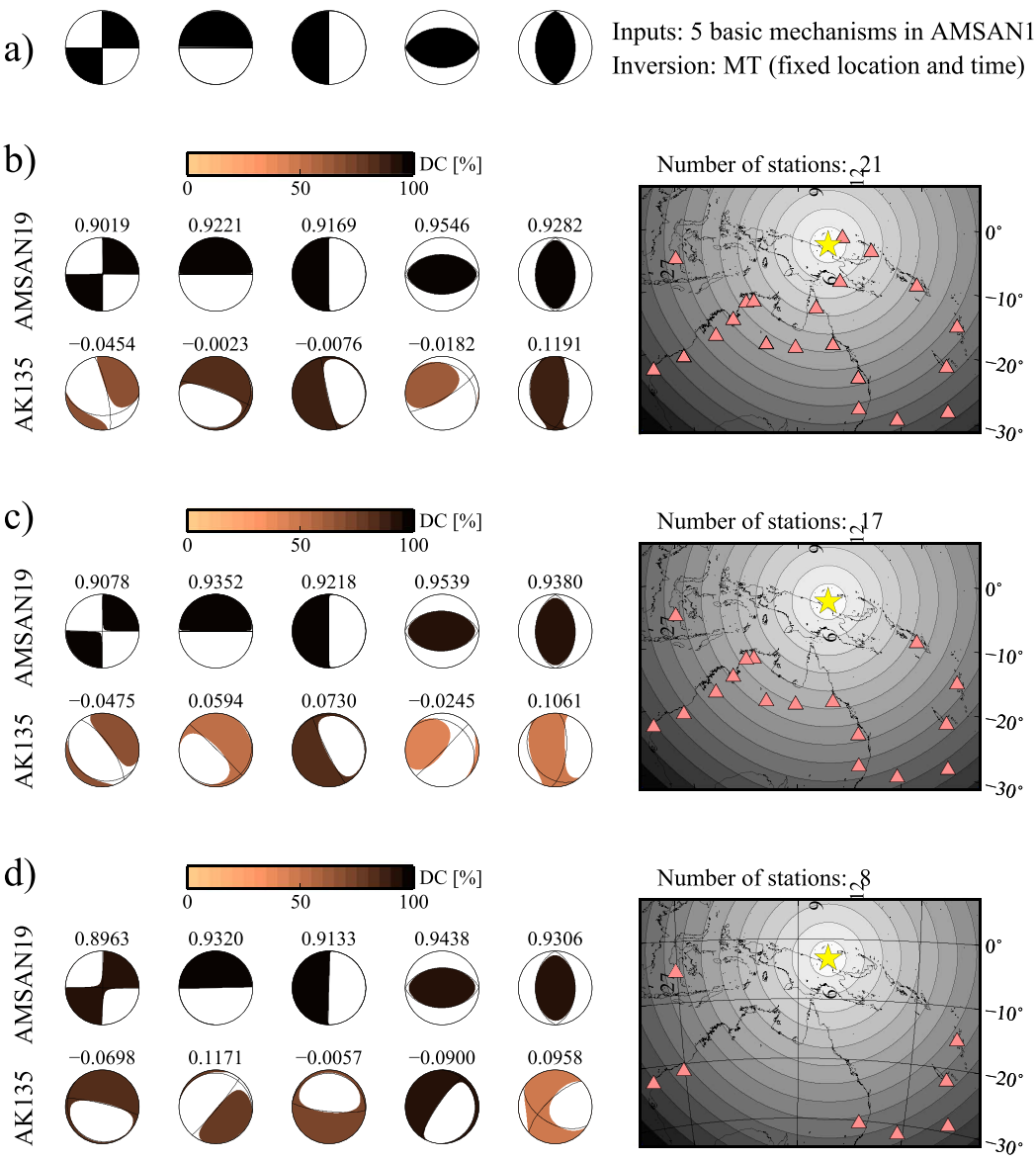

Figure 6. Synthetic recovery tests for five basic mechanisms in the ak135 and AMSAN19 models located at latitude −3.2°, longitude 145.0°, and depth 7 km. In this inversion, time and location of the event is fixed at the true value. (a) Five mechanisms used to generate "real data" in the AMSAN19 Earth model. Inversion using (b) 21 stations, (c) 17 stations at distances larger than 15°, and (d) eight stations at distances larger than 24°. The top line of beach balls shows the recovery in AMSAN19, and the bottom line shows the recovery using the ak135 synthetics. The location of the event (yellow star) and the stations (red triangles) is shown on the right. The variance reduction between the "real' and synthetic data is written on top of each beach ball.

first basis M_1) and the recovered mechanisms (strike, dip, and rake) are more similar to that of the input, compared to the previous tests. Moreover, the variance reduction increases by about 5–10%. These improvements indicate a trade-off between the correct MT components and correct time shift caused by the heterogeneities in the 3-D model. The first basis MT, M_1, is now recovered as a strike-slip mechanism, but the DC percentage is only 17. This is a clear sign that ignoring the 3-D heterogeneity in the synthetic Green's functions can readily translate into significant spurious non-DC components even in the presence of good azimuthal coverage and a well-known location and depth for the event. Using stations at larger distances, both mechanism and DC percentage became highly inaccurate (similar to that shown in Figure 6). AMSAN19 provides the same results as in case 1.

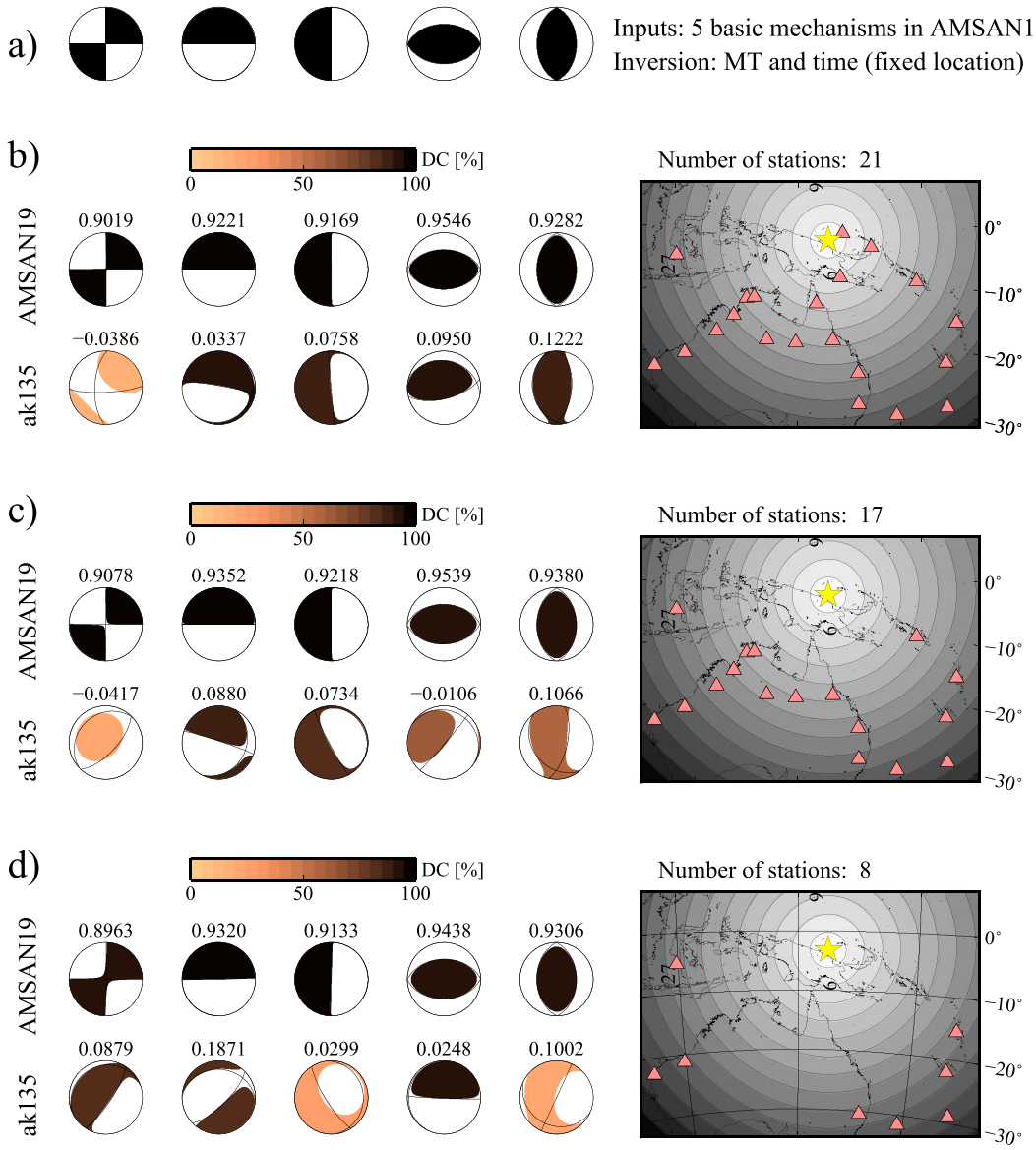

Figure 7. Synthetic recovery tests for five basic mechanisms in the ak135 and AMSAN19 models located at latitude −3.2°, longitude 145.0°, and depth 7 km. In this inversion, location of the event is fixed at the true value. (a) Five mechanisms used to generate "real data" in the AMSAN19 Earth model. Inversion using (b) 21 stations, (c) 17 stations at distances larger than 15°, and (d) eight stations at distances larger than 24°. The top line of beach balls shows the recovery in AMSAN19, and the bottom line shows the recovery using the ak135 synthetics. The location of the event (yellow star) and the stations (red triangles) is shown on the right. The variance reduction between the "real" and synthetic data is written on top of each beach ball.

3.3. Case 3: 4-D Search for Centroid Moment Tensor (Figure 8)

At periods greater than 40 s, the ground motion for a shallow source is relatively insensitive (nearly zero-amplitude seismograms) to M_2 and M_3 (vertical dip slip) and the shapes of the synthetics for the rest of the elementary basis are almost identical [*Dziewonski et al.*, 1981]. Consequently, a good compromise for the GCMT method is to fix the depth at 12 km for the centroids that tend to become shallower than this depth.

For the final synthetic test, we performed a full spatiotemporal grid search for the CMT. Two plots through the grid search summarize the effect of incomplete Earth structure (1-D model) on location, time, mechanism, and DC%, when they are all searched together (Figure 8). The recovery of centroid depth, time and

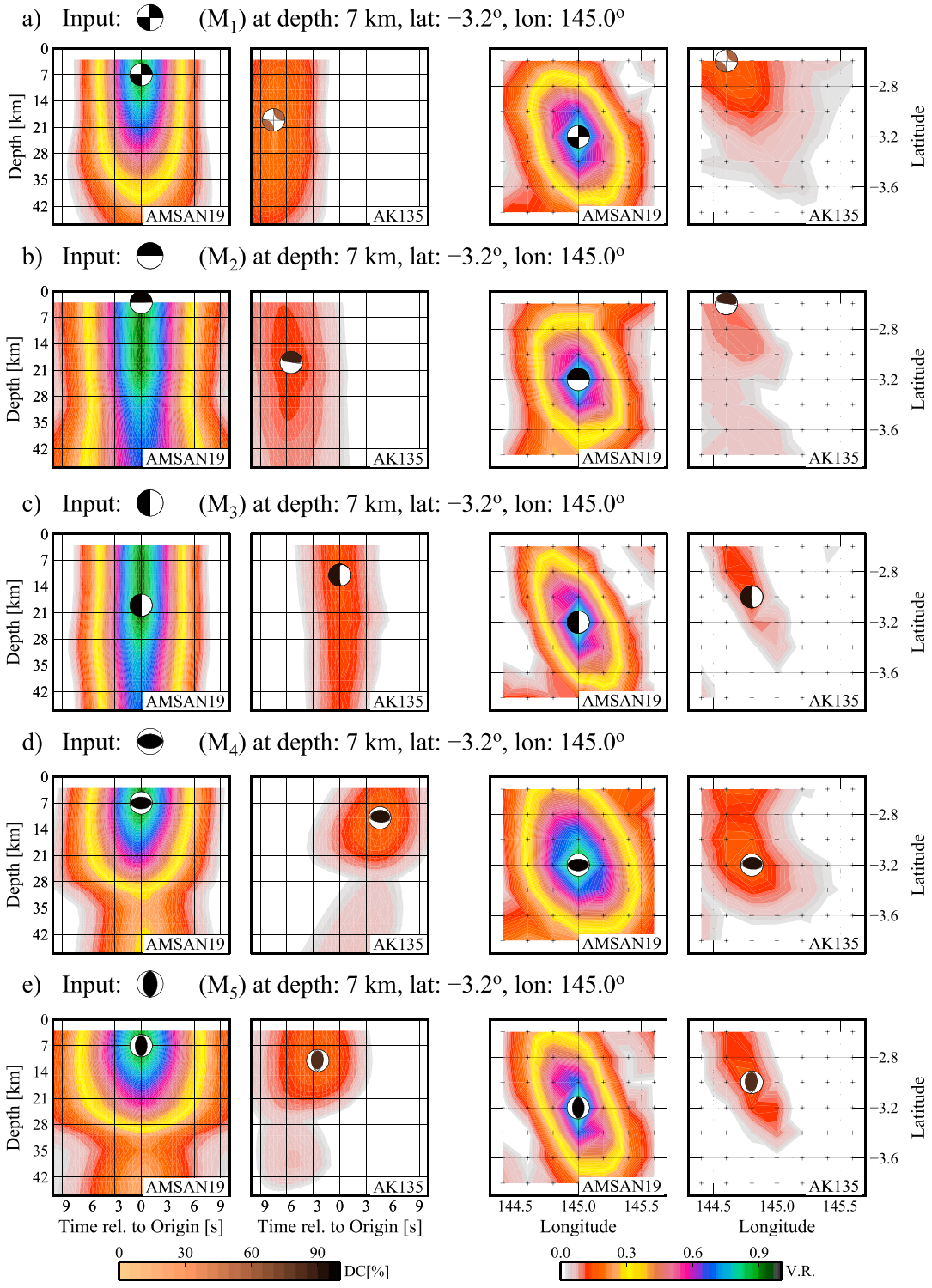

Figure 8. This synthetic test investigates the effect of 3-D heterogeneity on CMT solution of the basic mechanisms for a shallow earthquake. Similar to Figure 6, five mechanisms (Figure 6a) were used to simulate "real data" in the AMSAN19 Earth model for 21 stations (location of the stations is shown in Figure 6b). Inversion is performed using ak135 and AMSAN19 models. We did not add noise to the real data, so the differences in inversion results are fully related to the heterogeneity of the 3-D model. We present the result of CMT solution through the contour plot of variance reduction for (left) depth-time and (right) horizontal location in each model for (a) M_1, (b) M_2, (c) M_3, (d) M_4, and (e) M_5. Each beach ball is plotted with the DC percent as color (similar to Figures 5 and 7). The contour map of variance reduction is plotted with a different color bar in the background.

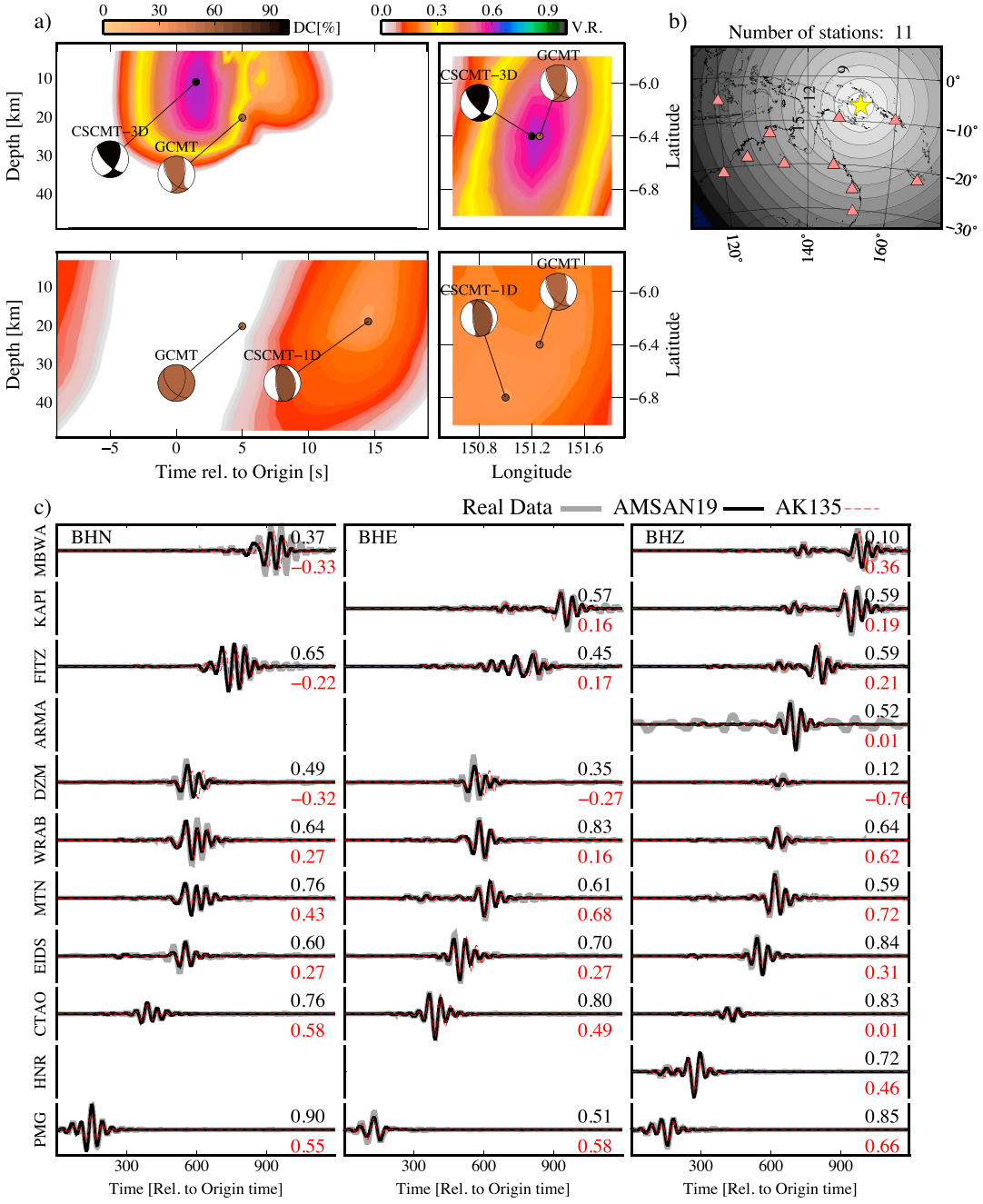

Figure 9. CMT solution for the event occurred on 12 November 2006 18:21:30 with M_w 6.2. The presentation of variance reduction and DC percent is similar to Figure 8. (a) Contour map of the depth, time, and horizontal location optimization for AMSAN19 and ak135 models. (b) Location of the earthquake (yellow star) and the 11 stations (red triangles) used. (c) Waveform fit between the observed data (thick gray), and the synthetics calculated from AMSAN19 (thinner black line) and ak135 (dashed red lines). (left) N-S components, (middle) E-W components, and (right) vertical components are shown. The seismograms are in velocity (m/s) units.

location (correct depth is 7 km, correct location is the center of the horizontal slice, and the correct time is zero) is shown by contouring variance reduction on a depth-time plot as well as a horizontal grid stencil at optimum depth.

When 1-D synthetics are used, M_4 and M_5 are only weakly sensitive to the depth (almost the same fit is achieved for the depths 3–21 km), whereas M_1, M_2, and M_3 are completely insensitive to the depth. The horizontal location has no clear peak, and instead, a large area with several local minima can be observed (with variance reduction up to 0.2). In general, there is a shift toward the north-west with maximum

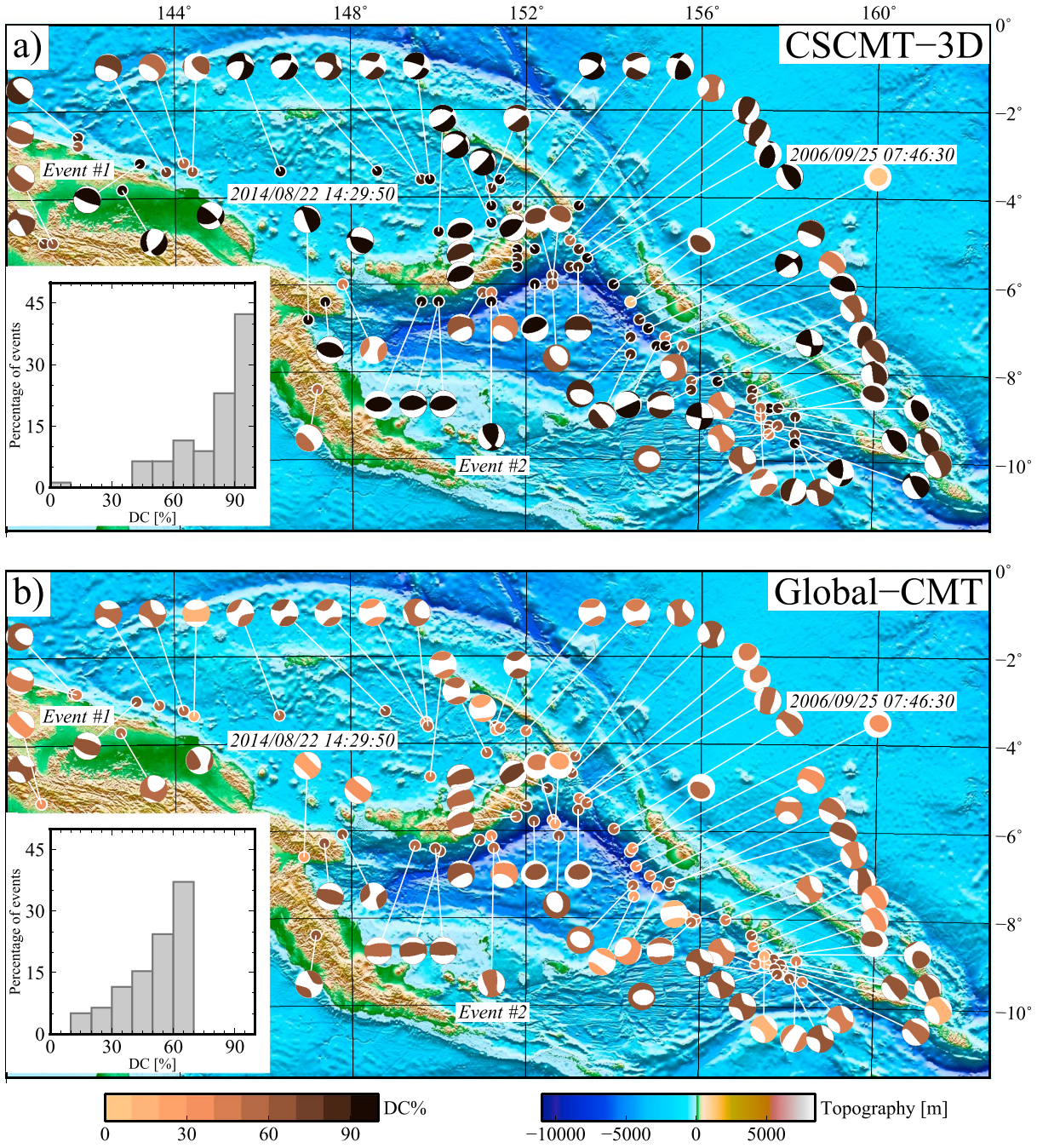

Figure 10. Topographic map of the study area with focal mechanism solutions obtained (a) using AMSAN19 model and (b) GCMT catalogue for events with DC% less than 70 in the GCMT catalogue. The histogram of the DC percentage is shown in insets in the bottom left corner of each map. Event #1, 12 November 2006 18:21:30 and event #2, 10 August 2009 17:46:23 are described in sections 4.1 and 4.2, respectively.

dislocation of 72 km (located at the edge of the stencil of grid points for M_1 and M_2). This indicates that the location and depth cannot always be well constrained using a 1-D Earth model, even in the presence of a reasonable azimuthal coverage.

In this test, using the 1-D synthetics, the optimum mechanisms are similar to the input mechanism (see Figures 6b and 7b for a comparison), which shows that there is a significant trade-off between the correct lateral location, depth, and time with MT components. The differences in the Green's functions and time delays stemming from the 3-D heterogeneity could also be partially compensated by a shift in the CMT location and time.

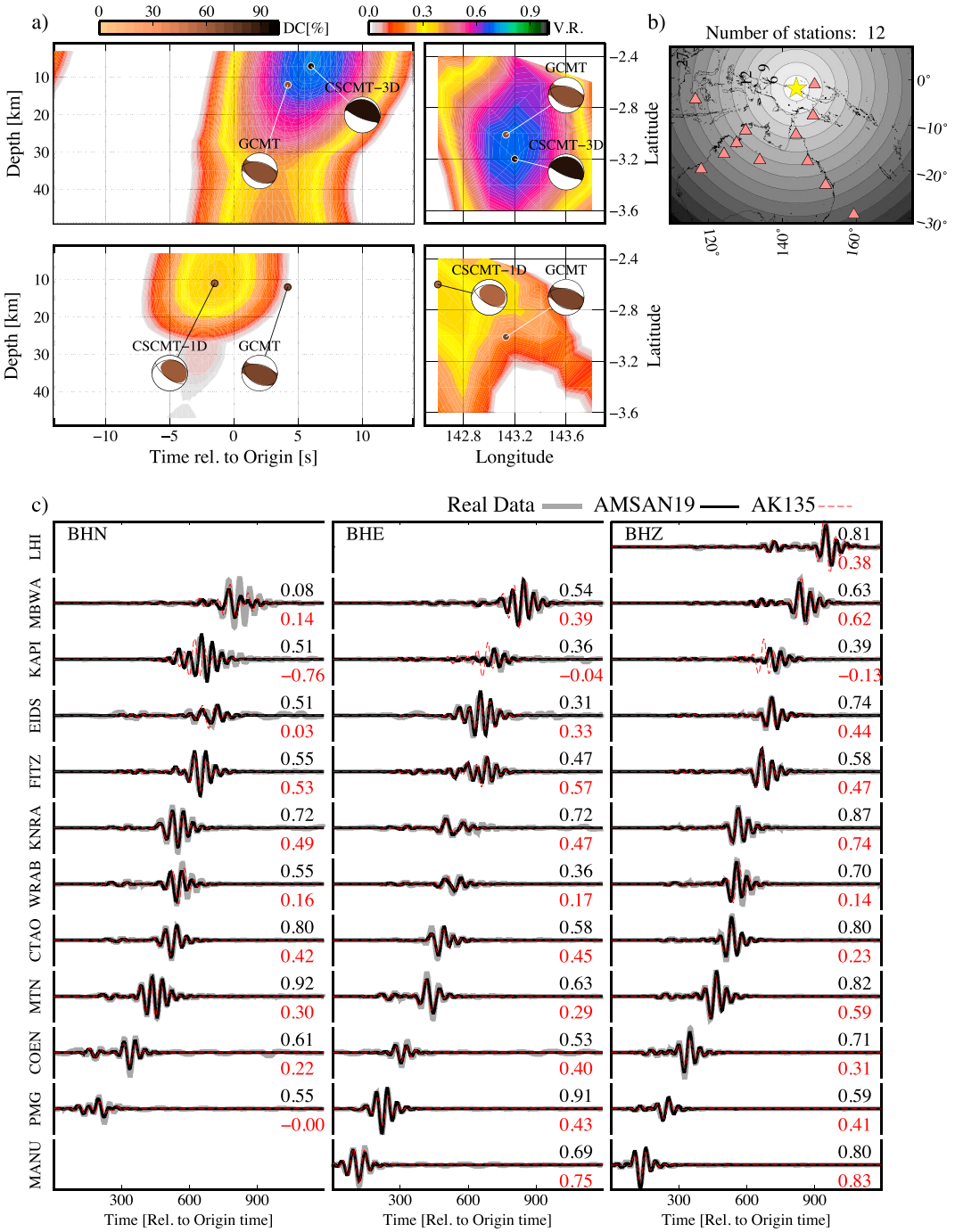

Figure 11. CMT solution for the event occurred on 10 August 2009 17:46:23 with M_w 5.7. The presentation of variance reduction and DC percent is similar to Figure 8. (a) Contour map of the depth, time, and horizontal location optimization for AMSAN19 and ak135 models. (b) Location of the earthquake (yellow star) and the 12 stations (red triangles) used. (c) Waveform fit between the observed data (thick gray), and the synthetics calculated from AMSAN19 (thinner black line) and ak135 (dashed red lines). (left) N-S components, (middle) E-W components, and (right) vertical components are shown. The seismograms are in velocity (m/s) units.

Using the 3-D synthetics, the time and lateral location of all elementary MTs are recovered correctly, with a strong peak in variance reduction. The depth recovery for M_1, M_4, and M_5 is a distinguishable peak at the correct depth, but M_2 and M_3 (vertical dip-slip mechanisms) show no depth sensitivity in the top 19 km.

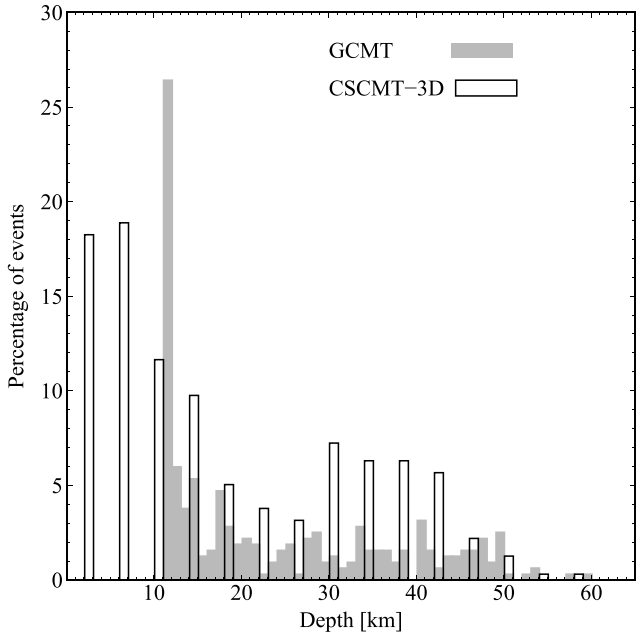

Figure 12. Histograms comparing centroid depths of earthquakes from the area of study CSCMT-3D (white) and GCMT (gray) catalogues.

Our synthetic tests confirm the known impact of 3-D structure on MT components for periods of 40–200 s on the continental scale [e.g., *Hingee et al.*, 2012]. Moreover, we observe a strong trade-off between centroid location and time with MT components when we use a 1-D Earth model. The 3-D heterogeneity affects the shape and arrival time of different phases, which can be partially compensated by a shift in the location, depth, and time of the centroid. Even in the presence of a good azimuthal coverage with stations distributed in a wide range of distances, incomplete knowledge of Earth structure can translate into significant spurious non-DC components. The discrepancies between true and recovered CMT solution become much more significant when we use less stations for the spatiotemporal grid search. Similar to the results shown in Figures 6 and 7, we repeated the CMT inversion using 17 and 8 stations. With the latter case, the error in lateral location is at least 100 km and reaches 50 km in depth. The shift in the recovered centroid time is larger than 10 s.

4. CMT Inversions for the Papua New Guinea, Bismarck Sea, and Solomon Islands

Data from 21 permanent broadband stations (14 operated by Geoscience Australia and 7 by GSN) were used to perform CSCMT inversions of 318 events with M_w~5.0 and larger that occurred in Papua New Guinea, the Bismarck Sea, and the Solomon Islands from 2006 to 2016 (Figure 1a). The maximum moment magnitude chosen for this study is M_w 7.4. Larger events were excluded to meet the requirements of a point source approximation for a finite source. We present two events in detail to describe the effect of 3-D heterogeneity on DC percentage, depth, location, and mechanism. These events summarize our main observations for the entire data set presented in the CSCMT catalogue.

4.1. Effect of 3-D Heterogeneity on DC Component; Event 1: 12 November 2006 18:21:30

About 24% of the events (78 earthquakes) in this study have DC% less than 70 in the GCMT catalogue. The MT from the GCMT catalogue for the event on 12 November 2006 18:21:30 located at the subducting New Guinea Trench has only 55% DC (Figure 9). We used data from 11 available broadband stations (Figure 9b) and two Earth models, AMSAN19 and ak135 to calculate the CSCMT-3D and CSCMT-1D.

The MT solution derived using ak135 shows similar DC (57%) but with different strike, dip, and rake angles compared to those reported by the GCMT. As expected, there is no clear optimum depth as the nodes at depth range of 10–50 km all produce similar fits to the data. The lateral location is not constrained well and the optimum centroid is located at ~60 km south-east of that reported by the GCMT (Figure 9a). In fact, an area with the size of 120 by 120 km produces more or less similar fits to the data as that of the optimum point. The optimum centroid time shows a 14 s shift relative to the hypocenter origin time (we used the same origin time as it was used by GCMT). According to empirical relations between the magnitude and the size of rupture as well as the source time function [*Somerville et al.*, 1999; *Tanioka and Ruff*, 1997] we argue that this is too large for an event with M_w 6.2 (reported by GCMT). Our CSCMT-1D solution estimates the moment magnitude to be 6.0.

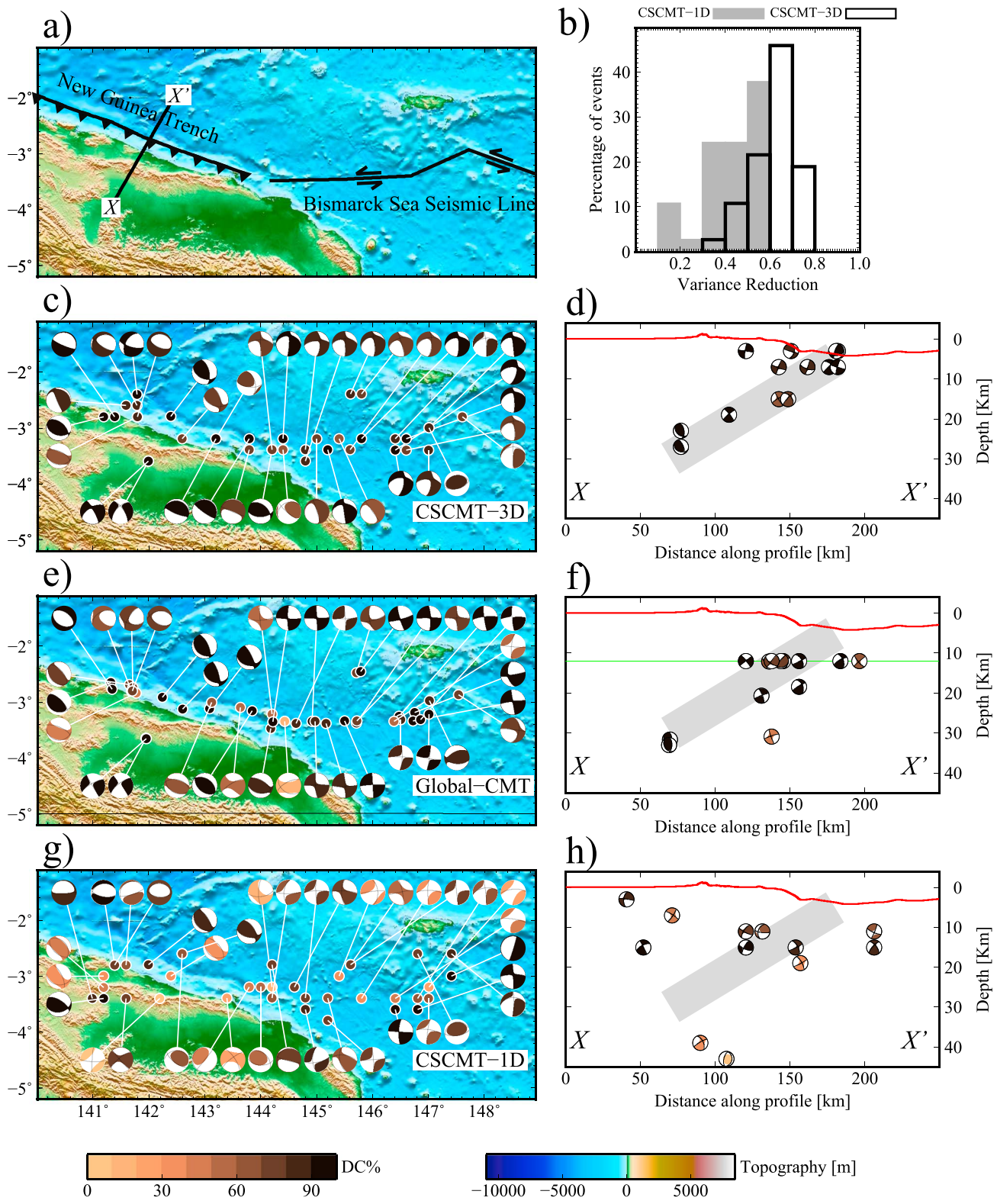

Figure 13. A comparison between CMT solutions in this study (CSCMT-3D and CSCMT-1D) and GCMT catalogue for 37 events occurred in north of Papua New Guinea along BSSL and New Guinea Trench. (a) Topography map, known faults, and the location of the cross section XX′, perpendicular to the New Guinea Trench. (b) Comparison between the fit to the data using AMSAN19 and ak135 models. The histogram of variance reduction is shown. (c) The CSCMT-3D solutions (map view), (d) projected on cross section XX′, (e) GCMT catalogue (map view), (f) projected on cross section XX′. (g) The CSCMT-1D solutions (map view), (h) projected on cross section XX′. On all cross sections, the red curve marks the topography along the profile XX′. The green line in cross section shown in Figure 13f indicates depth 12 km.

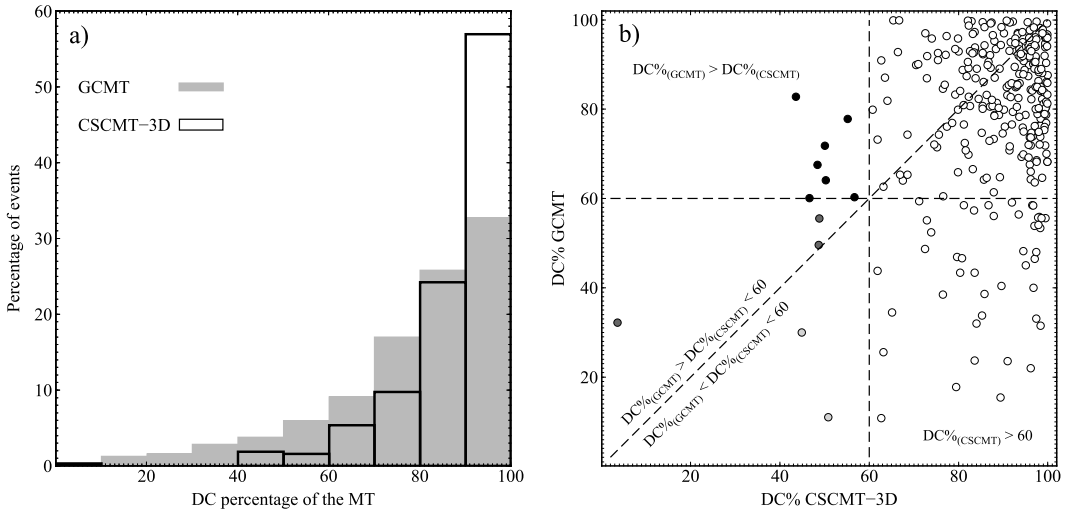

Figure 14. (a) A comparison between histograms of the DC% from CSCMT-3D (black line) and GCMT catalogues (filled dark gray). (b) Plot of DC% of GCMT solutions versus that of CSCMT-3D. Open circles indicate the events with DC >60% from CSCMT-3D catalogue. The light gray circles represent the solutions with DC <60% but with increase compare to GCMT. The black circles show the events for which DC% in CSCMT-3D catalogue is smaller than DC in GCMT catalogue.

For this event, using AMSAN19, the recovered mechanism and location are similar to that of GCMT; however, the DC part of the MT is 98%. The centroid location is optimized with a strong clear peak of variance reduction at longitude 151.2°E and latitude 6.4°S. The optimum depth is located between 11 and 20 km, and the centroid time is now 1.5 s after the origin time. The overall variance reduction increases from 0.19 using ak135 to 0.61 using AMSAN19 (Figure 9c), and moment magnitude increases by 0.1 compared to that of ak135. The angle ω_{9D} is 20°. Since the strike, dip, and rake of CSCMT-3D and GCMT mechanisms are very similar, ω_{9D} mainly represents the difference in non-DC components of the MTs.

It is evident that synthetics constructed using the 3-D model fit the observed data much better and enable us to locate the event with a localized peak of variance reduction. Moreover, the CSCMT-3D shows similar mechanisms to that of the GCMT but with 43% higher DC. This event represents a considerable portion of the events in the GCMT catalogue with significant non-DC components.

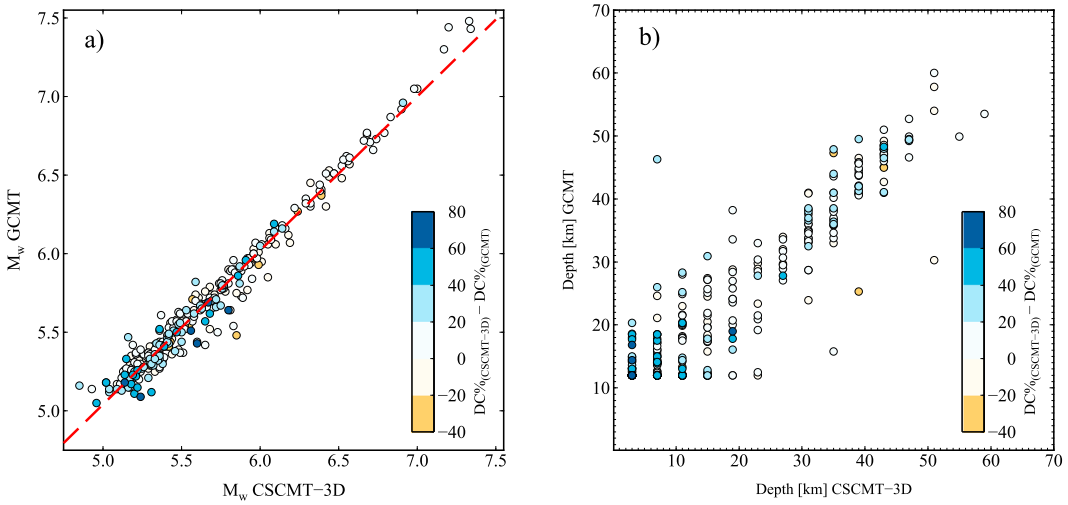

Figure 15. (a) Plot of moment magnitude from the CSCMT-3D catalogue versus that of GCMT catalogue. The color bar is the difference between the DC percentages in two data sets. The dashed red line is the best linear fit to the data. The correlation coefficient is 0.98. (b) Same as in Figure 15a but for depth parameter.

Table 1. CSCMT-3D Results for 318 Earthquakes[a]

Number	Origin Time	Longitude	Latitude	Depth	Mrr	Mtt	Mff	Mrt	Mrf	Mtf	Exp	M_w	DC%
1	20060206030402	149.8	−6.4	35	2.86	−2.83	−0.03	1.14	0.17	0.02	17	5.6	97.4
2	20060317134814	150.0	−4.8	11	−2.93	3.81	−0.88	−1.79	−2.49	1.05	17	5.7	96.8
3	20060320141757	151.4	−6.0	27	1.76	−0.22	−1.54	−0.52	0.24	0.77	17	5.4	94.4
4	20060324122709	143.2	−3.2	3	7.65	−5.29	−2.36	6.74	5.21	8.99	17	6.0	75.4
5	20060529121213	154.8	−7.8	7	−0.15	1.29	−1.14	0.69	−0.57	0.36	17	5.4	95.8
6	20060601131625	151.8	−5.2	43	9.63	−8.84	−0.78	3.01	0.92	−2.24	16	5.3	96
7	20060823231521	152.8	−4.2	35	−2.27	1.36	0.90	0.32	−1.69	−0.88	17	5.5	62.7
8	20060901101853	155.4	−7.0	39	1.52	−0.90	−0.62	0.00	−0.04	0.75	19	6.7	100
9	20060905213851	145.8	−3.2	7	−2.02	0.18	1.84	1.23	−5.30	5.44	16	5.1	92.2
10	20060915101317	150.4	−6.4	31	5.21	−5.16	−0.05	2.98	1.04	−0.77	17	5.8	99.5
11	20060925074630	154.4	−6.4	43	2.02	−1.07	−0.96	0.17	−0.37	−0.02	17	5.4	3.6
12	20061017085825	151.4	−6.0	31	1.90	−0.64	−1.26	0.11	0.02	−0.42	17	5.4	55.2
13	20061018020914	151.2	−6.2	3	0.36	−0.32	−0.04	1.74	0.68	−0.04	17	5.4	94.6
14	20061030042917	154.8	−6.8	35	1.40	−0.84	−0.56	0.46	−0.20	0.80	17	5.4	88.1
15	20061112103511	151.6	−6.6	3	−8.05	4.17	3.88	2.55	1.93	2.37	16	5.2	61.9
16 (#1)	20061112182130	151.2	−6.4	11	0.90	0.90	−1.80	0.98	−0.16	0.45	18	6.1	98.1
17	20061119091944	151.6	−6.4	3	−8.49	6.00	2.49	0.78	4.94	3.88	16	5.2	76.5
18	20061207110132	154.2	−6.2	39	8.98	−5.14	−3.84	−0.12	3.39	5.33	16	5.2	95.5
19	20061218234615	154.6	−7.0	7	6.45	−3.64	−2.81	3.49	−1.23	2.74	16	5.1	82.9
20	20070122192550	146.4	−3.2	11	−1.11	−0.94	2.05	0.55	−3.14	3.94	17	5.7	82.1
21	20070213105657	154.6	−7.0	11	5.09	−3.15	−1.94	7.65	−5.30	3.01	16	5.2	90.9
22	20070217091834	156.0	−7.4	11	7.26	−5.60	−1.67	2.69	−1.84	2.76	16	5.2	93.3
23	20070217124312	155.8	−7.6	7	1.88	−1.93	0.05	0.30	−0.88	0.68	17	5.5	98.7
24	20070217074334	156.0	−7.6	15	3.49	−2.67	−0.82	1.02	−0.78	1.02	17	5.6	79.3
25	20070304025006	152.6	−6.0	3	−9.13	3.18	5.95	−7.85	8.04	−1.97	16	5.3	67.5
26	20070402134953	156.4	−8.2	11	0.34	−0.04	−0.30	0.49	0.45	1.77	17	5.4	94.5
27	20070402224950	154.8	−9.8	3	−2.52	2.29	0.22	2.26	0.45	0.17	17	5.6	87.1
28	20070402104919	156.2	−7.6	43	1.21	−0.73	−0.48	−0.39	0.20	0.56	18	6.0	93.6
29	20070402232023	157.4	−9.0	11	2.00	−1.43	−0.56	1.29	−0.17	0.74	18	6.1	82.2
30	20070402120223	157.8	−8.8	11	1.92	−0.41	−1.51	−0.47	−0.59	1.27	18	6.1	87.9
31	20070403213454	158.2	−9.0	19	4.28	−1.32	−2.96	5.50	0.50	4.89	16	5.1	89.4
32	20070403024637	155.6	−7.4	7	−3.13	6.63	−3.51	1.54	−5.69	2.27	16	5.2	50.8
33	20070403052116	157.4	−8.8	7	4.02	−0.05	−3.97	0.53	−9.20	3.83	16	5.2	85.8
34	20070403172556	157.6	−8.8	15	1.14	−0.30	−0.84	−0.36	−0.35	0.70	17	5.3	96.2
35	20070403152706	155.4	−7.6	7	1.31	−0.95	−0.36	0.71	−0.36	0.56	17	5.4	96.2
36	20070403002207	154.8	−10.0	3	−1.42	1.29	0.13	−0.03	0.46	0.04	17	5.4	66.9
37	20070403221741	154.8	−7.0	19	1.71	−1.05	−0.66	0.70	−0.66	0.80	17	5.4	96
38	20070403194057	155.2	−7.2	23	1.09	−0.64	−0.45	1.23	−0.77	1.19	17	5.4	48.8
39	20070403120427	155.8	−8.4	3	−1.03	1.27	−0.24	−0.60	0.37	0.21	18	6.0	86.7
40	20070404094613	155.0	−7.2	11	8.91	−5.77	−3.15	9.60	−5.66	3.01	16	5.3	83.6
41	20070404093556	154.8	−7.2	23	1.51	−1.00	−0.51	1.14	−0.79	0.67	17	5.4	95.8
42	20070404003950	156.0	−7.4	47	9.43	−5.71	−3.73	−2.17	0.47	4.81	17	5.9	98.1
43	20070404063436	156.6	−7.8	19	3.46	−1.06	−2.40	0.07	−1.11	1.66	18	6.3	98.7
44	20070406091218	157.2	−8.6	11	1.15	−0.59	−0.57	0.59	−0.38	0.59	17	5.3	99.6
45	20070414231657	145.0	−3.4	7	−4.00	0.42	3.58	2.12	−8.74	6.90	16	5.2	86.3
46	20070424121424	155.8	−8.0	7	−2.84	8.97	−6.13	−1.00	−3.77	−2.31	16	5.2	91.7
47	20070427134927	155.8	−7.4	43	6.33	−3.91	−2.42	−0.55	0.43	2.54	17	5.8	83.8
48	20070429034430	157.2	−8.4	11	1.02	0.06	−1.07	−0.46	−0.91	0.18	17	5.3	85.7
49	20070501001522	155.0	−7.4	3	−0.52	1.77	−1.25	−7.73	−3.64	−0.84	17	5.8	98.4
50	20070501014524	155.2	−7.6	3	0.34	−0.20	−0.14	1.27	−0.23	0.11	18	5.9	85.6
51	20070510111508	155.2	−7.4	31	1.56	−1.36	−0.20	1.13	−0.17	0.58	17	5.4	99.9
52	20070518231126	152.0	−7.2	27	−0.28	−1.60	1.87	−1.82	0.59	−3.63	17	5.6	85.4
53	20070601192205	149.2	−3.4	11	−0.31	0.91	−0.60	−0.22	−1.73	1.25	17	5.4	82.3
54	20070607004040	147.0	−3.0	19	0.21	−0.32	0.10	0.21	−2.54	2.14	18	6.2	93.3
55	20070616042359	155.4	−7.6	3	3.64	−3.72	0.07	7.16	−6.72	1.51	17	5.9	98.4
56	20070618061848	151.2	−3.6	7	−2.44	3.73	−1.28	−1.05	−2.19	1.01	18	6.3	93.7
57	20070628025210	154.8	−7.8	3	0.04	0.68	−0.71	1.43	−1.21	0.17	19	6.7	97
58	20070722154211	141.8	−2.6	7	−4.48	5.76	−1.28	−4.75	4.59	−0.38	16	5.2	86.3
59	20070722142044	141.8	−2.8	7	−2.94	2.55	0.39	−2.69	1.52	−0.43	17	5.6	79.9
60	20070722104938	141.8	−2.4	3	−1.70	3.07	−1.37	−1.94	1.61	2.10	17	5.6	96.6
61	20070806002631	141.6	−2.6	3	1.05	−0.49	−0.56	0.93	−2.49	0.96	17	5.5	87.9

Table 1. (continued)

Number	Origin Time	Longitude	Latitude	Depth	Mrr	Mtt	Mff	Mrt	Mrf	Mtf	Exp	M_w	DC%
62	20070815165144	155.8	−7.4	15	1.08	−0.76	−0.32	0.38	−0.32	0.49	17	5.3	99.6
63	20070819190943	141.0	−5.0	11	2.83	−5.24	2.41	1.86	−6.26	7.13	16	5.2	76.6
64	20070820213045	141.2	−5.0	3	2.45	−1.20	−1.25	−5.10	3.65	2.70	17	5.8	65.1
65	20070826134705	154.2	−10.0	3	−9.31	6.65	2.65	8.91	6.88	2.69	16	5.3	80.4
66	20070926123626	153.6	−5.2	43	1.29	−0.40	−0.89	0.00	0.07	0.61	19	6.7	98.7
67	20071021102452	154.4	−6.8	39	6.20	−4.18	−2.02	−0.06	1.57	3.84	17	5.8	82.3
68	20071022061112	141.4	−2.8	3	−1.50	1.13	0.37	−4.45	1.86	−0.65	17	5.7	99.4
69	20071026163444	143.8	−3.4	3	0.48	−2.03	1.55	8.95	−3.60	0.68	17	5.8	71.2
70	20071101000520	153.6	−5.2	43	1.56	−0.51	−1.05	0.24	−0.30	0.72	17	5.4	98.4
71	20071101214539	154.8	−6.8	11	1.27	−0.77	−0.49	1.57	−1.08	0.67	17	5.4	96.2
72	20071116075220	151.8	−5.8	15	6.62	−5.76	−0.86	7.29	1.00	−2.80	16	5.2	98.4
73	20071120125259	155.8	−7.2	51	1.08	−1.08	−0.01	−0.18	0.28	0.07	18	6.0	89.1
74	20071124134838	152.2	−4.2	7	−0.78	1.35	−0.57	−0.57	−0.81	0.26	17	5.4	90.4
75	20071203223312	148.8	−6.8	15	2.72	−2.73	0.01	2.03	−0.13	−0.09	17	5.6	99.7
76	20071210121328	144.4	−3.4	3	0.67	−1.20	0.53	0.92	−1.33	−0.06	17	5.4	62.7
77	20080101191308	147.2	−6.0	43	4.82	−3.93	−0.89	0.64	−1.20	1.62	17	5.7	87.4
78	20080203171024	149.8	−6.6	35	1.17	−1.24	0.07	0.49	0.04	0.02	17	5.3	89.9
79	20080314095903	141.6	−3.2	15	4.25	−4.18	−0.06	−1.23	0.68	1.96	16	5.0	72.5
80	20080319115552	155.4	−7.2	23	8.17	−6.86	−1.32	6.41	−3.16	4.86	16	5.3	75.6
81	20080503190145	155.2	−6.6	31	3.43	−2.23	−1.20	0.64	−0.92	1.66	17	5.6	99.6
82	20080524132408	156.0	−7.4	39	2.45	0.67	−3.12	−1.27	−3.66	5.37	17	5.8	84.5
83	20080622131535	157.8	−9.4	11	6.19	−3.15	−3.04	2.62	−5.28	3.88	16	5.2	90.8
84	20080622072205	157.8	−9.2	11	4.57	−2.11	−2.47	1.27	−2.59	2.56	17	5.7	94.1
85	20080625154128	151.8	−5.6	47	3.55	−3.39	−0.16	0.52	−0.05	−0.74	17	5.6	99.6
86	20080711095851	148.2	−3.2	7	−0.49	1.54	−1.05	−0.08	−1.71	2.04	17	5.5	92.2
87	20080720211338	151.4	−3.8	7	0.02	1.78	−1.80	−1.82	−1.20	−0.57	17	5.5	93.1
88	20080725201107	146.8	−6.0	47	1.78	−1.46	−0.33	0.06	0.14	0.60	17	5.4	91.4
89	20080826020626	147.6	−2.8	7	−0.07	−0.15	0.22	−0.10	−1.39	0.76	17	5.3	75.2
90	20080909122250	158.2	−9.6	7	3.45	0.95	−4.40	2.98	4.59	7.50	17	5.9	97.1
91	20081022045151	155.0	−7.4	3	7.17	−4.32	−2.86	8.65	−8.71	2.51	16	5.3	85.4
92	20081023111530	145.6	−2.4	11	−2.60	−0.46	3.07	2.24	−6.64	5.24	16	5.2	81.2
93	20081023100436	145.8	−2.4	11	−0.17	−1.36	1.53	1.24	−2.17	2.49	18	6.2	72.6
94	20081101011310	149.2	−3.2	15	−2.13	6.11	−3.98	−2.82	−9.29	6.62	17	5.9	99.6
95	20081217080957	148.0	−7.2	7	0.00	0.26	−0.26	−0.78	1.24	−0.09	17	5.3	95.7
96	20090108214704	153.0	−4.8	35	−0.01	6.28	−6.27	−3.18	−1.60	−4.20	16	5.2	98.3
97	20090208153437	147.8	−6.4	35	2.53	−2.21	−0.33	0.82	−0.05	0.52	17	5.5	85.2
98	20090214202911	151.8	−5.6	35	1.20	−1.13	−0.07	0.52	0.10	−0.27	17	5.3	99.3
99	20090303011937	151.4	−3.8	7	−0.76	1.46	−0.70	−0.48	−1.00	0.39	17	5.4	99.3
100	20090322193420	151.8	−5.4	31	9.86	−9.44	−0.42	6.10	2.73	−4.20	16	5.3	81.2
101	20090322193420	151.8	−5.6	35	1.21	−1.07	−0.13	0.51	0.13	−0.42	17	5.3	96.5
102	20090324232827	151.8	−5.4	43	5.42	−4.95	−0.47	1.81	0.83	−1.01	17	5.8	90.2
103	20090401035501	144.4	−3.2	3	−0.56	0.98	−0.42	−0.15	−6.30	4.10	18	6.4	90.2
104	20090415182633	154.0	−6.2	31	8.78	−2.74	−6.05	−2.93	−0.40	3.90	16	5.2	81.8
105	20090416004324	154.2	−6.8	3	2.77	−1.17	−1.60	9.25	−6.26	0.99	17	5.9	90.9
106	20090530195643	149.8	−6.6	15	5.07	2.08	−7.15	4.09	−2.73	2.78	16	5.2	77.4
107	20090604010342	146.6	−6.2	31	7.96	−8.30	0.34	5.21	−4.22	0.77	16	5.3	87.2
108	20090715201043	150.6	−3.4	15	−0.61	1.26	−0.65	0.59	−0.78	1.41	18	6.1	97.5
109	20090725014224	155.0	−6.8	39	6.81	−3.69	−3.11	0.54	−1.02	3.83	17	5.8	88.6
110	20090727123418	151.8	−5.8	19	6.34	−7.16	0.82	5.65	−0.66	−2.10	16	5.2	81.4
111	20090729213304	152.8	−5.4	27	1.09	−1.09	0.00	1.20	0.17	−0.15	17	5.4	97.3
112 (#2)	20090810174625	143.2	−3.2	7	3.26	−3.03	−0.23	4.65	−1.97	1.14	17	5.7	94.5
113	20090817152103	154.6	−6.8	3	0.18	−0.28	0.10	1.46	−0.63	0.11	17	5.3	85.3
114	20090818175915	154.6	−6.8	7	0.77	−0.20	−0.57	1.10	−2.14	0.34	17	5.5	99.9
115	20090922043809	142.0	−3.6	27	−0.90	−1.46	2.36	1.07	−0.43	0.34	17	5.5	93.5
116	20091009224956	157.6	−9.4	7	1.38	−1.10	−0.28	0.50	−1.80	1.22	17	5.5	97.8
117	20100103041140	146.0	−5.4	43	5.05	−0.88	−4.18	1.96	−2.97	1.98	17	5.8	99.4
118	20100103214804	157.6	−9.0	7	7.76	−2.66	−5.10	4.79	−5.69	2.91	18	6.6	85.8
119	20100103223629	157.4	−8.8	7	3.47	−1.33	−2.13	1.80	−2.90	1.39	19	7.0	88
120	20100104142419	157.2	−8.6	15	7.36	−2.29	−5.08	3.45	−2.67	4.79	16	5.2	76.5
121	20100104041748	157.6	−9.2	7	1.88	−0.67	−1.22	0.71	−1.04	0.90	17	5.5	99.9
122	20100104112821	157.2	−8.6	7	3.84	−2.26	−1.59	4.58	−2.76	2.08	17	5.8	96.7

Table 1. (continued)

Number	Origin Time	Longitude	Latitude	Depth	Mrr	Mtt	Mff	Mrt	Mrf	Mtf	Exp	M_w	DC%
123	20100105131143	157.8	−9.4	7	5.64	−3.10	−2.54	4.88	−4.06	2.71	17	5.8	97.7
124	20100105121534	157.8	−9.2	11	1.29	−0.73	−0.56	0.45	−0.59	0.69	19	6.7	95
125	20100109070432	157.6	−9.4	7	3.00	0.98	−3.99	−0.05	−2.50	8.18	16	5.2	46.6
126	20100109055133	157.8	−9.2	7	0.21	0.26	−0.48	0.55	0.37	2.28	18	6.1	98.7
127	20100117094642	152.8	−6.2	3	−2.26	2.28	−0.02	−1.53	−0.05	−0.27	17	5.5	97.1
128	20100119001748	158.2	−9.0	3	−2.59	0.63	1.96	0.65	3.75	1.92	17	5.7	89.6
129	20100124141900	157.8	−9.2	7	0.23	−0.03	−0.20	−0.14	0.86	1.45	17	5.3	68.6
130	20100201222817	154.4	−6.4	35	1.82	−0.87	−0.96	0.59	−0.03	1.03	18	6.1	96.5
131	20100210071834	154.8	−7.4	3	0.93	−0.52	−0.42	3.51	−2.52	0.34	17	5.6	94.3
132	20100312032249	157.6	−9.2	7	0.60	3.02	−3.62	−0.56	−0.33	7.43	16	5.1	87.1
133	20100410061613	145.8	−4.8	11	−5.43	−0.98	6.41	3.86	−4.93	7.71	16	5.2	98.9
134	20100602092854	149.4	−6.4	35	7.83	−7.83	0.00	1.27	1.83	−1.17	17	5.9	96.3
135	20100619112246	150.6	−3.2	11	−0.63	1.15	−0.52	−0.51	−0.62	0.02	17	5.3	91.5
136	20100620102133	146.8	−6.2	47	1.24	−1.02	−0.21	−0.15	0.05	0.27	17	5.3	78.6
137	20100707091335	154.4	−6.4	31	1.07	−0.41	−0.65	0.26	−0.13	0.46	17	5.3	86.7
138	20100718130411	150.6	−6.4	31	2.85	−0.01	−2.83	−0.18	−0.26	−0.39	19	6.9	97.9
139	20100718133460	150.4	−6.2	35	6.74	−6.90	0.16	3.23	1.00	0.13	19	7.2	99.4
140	20100719030111	150.2	−6.8	15	6.76	−6.26	−0.50	5.05	−1.31	−0.46	16	5.2	83.7
141	20100720235433	141.2	−2.8	19	6.30	−5.08	−1.22	−0.42	1.87	2.91	16	5.1	99.4
142	20100720203108	150.4	−6.4	27	1.40	−1.26	−0.13	0.46	0.00	−0.47	17	5.4	97
143	20100720191822	150.8	−6.4	35	3.29	−3.24	−0.05	1.15	−0.18	−0.38	18	6.3	98.3
144	20100731042820	150.4	−6.4	27	0.71	0.53	−1.24	0.42	−0.37	−0.04	17	5.3	66.4
145	20100804220143	150.8	−6.2	31	2.16	−2.11	−0.05	0.92	−0.01	−0.39	19	6.8	99.1
146	20100805050922	150.4	−6.6	31	0.99	−1.08	0.09	0.34	−0.08	−0.17	17	5.3	82.6
147	20100805050922	150.4	−6.4	31	1.02	−1.07	0.05	0.33	−0.08	−0.21	17	5.3	87.6
148	20100814103559	151.0	−6.2	39	1.23	−1.08	−0.15	0.26	−0.01	−0.18	17	5.3	81.1
149	20100820084733	154.2	−6.8	3	0.86	−0.40	−0.46	2.16	−1.65	0.33	17	5.5	91.5
150	20100820175615	154.2	−6.8	3	0.98	−0.41	−0.58	2.65	−1.82	0.39	18	6.2	90.8
151	20100903022910	150.0	−6.4	31	1.61	−1.65	0.05	0.53	0.19	−0.07	17	5.4	96.2
152	20100923125308	151.8	−6.2	15	2.11	−1.91	−0.19	1.35	0.15	−0.34	17	5.5	89.6
153	20101005192203	151.2	−3.8	11	−0.44	1.23	−0.79	−0.65	−0.87	0.16	17	5.4	99.2
154	20101021110030	151.0	−6.2	19	0.30	−0.97	0.67	1.37	0.70	−0.04	17	5.4	63.2
155	20101028031726	153.8	−5.6	51	1.06	−0.12	−0.94	1.72	−3.58	1.00	17	5.6	76.9
156	20101031163849	150.4	−6.6	7	−3.55	3.19	0.36	−3.37	0.22	−0.16	17	5.7	85.8
157	20101101051634	150.4	−6.8	35	5.06	−4.92	−0.13	7.60	−1.03	−3.22	16	5.2	96.9
158	20101102063955	151.6	−5.6	47	5.41	−5.11	−0.30	1.38	−0.09	−1.35	17	5.8	99.3
159	20101111202958	154.8	−6.4	43	1.91	−0.90	−1.00	0.16	0.60	1.02	17	5.5	92.8
160	20101202031209	149.8	−6.2	43	7.37	−7.82	0.45	2.46	2.09	0.07	18	6.5	97.8
161	20101212145310	150.2	−6.6	11	7.10	−7.04	−0.06	7.65	−2.58	0.31	16	5.2	93.6
162	20110216021537	149.4	−6.2	35	2.05	−2.09	0.05	0.30	0.23	0.03	17	5.5	98.3
163	20110304040748	157.4	−9.2	7	1.04	−0.41	−0.63	0.72	0.12	2.20	17	5.5	48.7
164	20110319161157	149.6	−6.4	43	8.44	−8.42	−0.03	0.21	−0.46	−0.50	16	5.2	99.5
165	20110430054535	148.8	−3.6	3	−0.54	3.00	−2.46	−1.61	−3.55	2.39	17	5.7	96
166	20110515232504	155.2	−7.0	7	0.84	−0.76	−0.09	1.04	−0.78	0.17	17	5.3	83.7
167	20110518185125	147.8	−6.6	7	−1.17	0.38	0.80	0.78	0.18	1.13	17	5.4	64.1
168	20110520194316	147.0	−7.4	3	−1.24	0.16	1.08	−7.70	3.79	−2.50	17	5.8	77.1
169	20110605070209	152.0	−3.8	3	−0.52	1.48	−0.97	−1.21	−1.22	−0.38	17	5.4	80
170	20110616000337	151.2	−6.2	11	−0.36	−1.25	1.61	2.87	−1.46	0.32	18	6.2	44.9
171	20110617031216	151.2	−6.4	3	−0.66	0.52	0.14	−1.17	0.99	−0.32	17	5.3	96.9
172	20110701162546	147.8	−6.8	3	−1.48	0.52	0.96	0.66	6.57	1.34	17	5.7	94.4
173	20110711002725	146.4	−3.4	7	−4.10	2.46	1.64	1.71	−5.33	6.69	16	5.2	93.1
174	20110725005050	150.6	−3.2	7	−0.93	3.64	−2.71	−1.42	−2.10	0.47	18	6.3	95.6
175	20110726174050	150.6	−3.2	11	−2.08	−0.72	2.80	2.44	−6.44	8.81	16	5.2	87.2
176	20110731233858	144.8	−3.6	7	−0.09	0.10	−0.01	0.98	−5.12	7.27	18	6.5	80.9
177	20110803223923	148.2	−5.0	3	2.94	−2.02	−0.92	−3.33	−0.25	2.73	17	5.7	97.4
178	20110810180615	155.6	−7.2	11	7.69	−5.20	−2.49	5.89	−2.76	2.99	16	5.2	88
179	20110812163036	148.6	−3.4	11	−5.21	7.55	−2.34	0.63	−6.31	7.35	16	5.3	98.2
180	20110821130408	151.0	−6.0	47	5.69	−5.53	−0.16	1.15	0.67	−0.88	17	5.8	98
181	20110831104648	153.2	−6.2	7	−2.70	0.69	2.01	−0.02	1.30	−0.51	17	5.6	63.5
182	20110912224430	144.2	−3.4	3	6.18	−6.34	0.16	1.63	2.17	2.65	17	5.8	99.2
183	20111003085749	152.6	−5.4	27	7.20	−6.76	−0.44	5.42	1.28	−1.00	16	5.2	93.5

Table 1. (continued)

Number	Origin Time	Longitude	Latitude	Depth	Mrr	Mtt	Mff	Mrt	Mrf	Mtf	Exp	M_w	DC%
184	20111014033515	148.4	−6.8	35	4.73	−1.06	−3.67	2.17	1.29	−1.83	18	6.4	85.5
185	20111018050506	151.0	−6.2	31	1.04	−1.01	−0.03	0.46	−0.06	−0.23	18	6.0	99.6
186	20111030021038	144.4	−4.6	19	5.47	−4.08	−1.38	−4.33	3.34	3.60	16	5.2	74.6
187	20111107044436	149.8	−3.6	15	−0.57	1.31	−0.74	−0.19	−0.87	0.54	17	5.4	96.2
188	20111120163140	142.4	−2.8	7	1.13	−0.41	−0.72	0.26	0.70	0.90	17	5.3	99.7
189	20111121034837	150.8	−3.2	15	−0.44	1.22	−0.77	0.07	−0.39	0.18	17	5.3	70.5
190	20111128122647	153.6	−5.8	31	1.53	−0.92	−0.61	0.89	−0.05	0.59	18	6.1	71
191	20120202093216	149.8	−6.8	7	−0.01	1.88	−1.87	0.60	−0.71	−0.76	17	5.5	92.7
192	20120314211310	151.0	−6.0	43	2.17	−2.00	−0.16	0.68	0.11	−0.36	18	6.2	91.7
193	20120404202730	152.2	−4.2	7	−0.90	0.86	0.04	−1.39	0.83	−0.27	17	5.4	99.6
194	20120428192103	152.2	−5.6	23	1.69	−1.55	−0.13	1.51	0.23	−0.66	17	5.5	92.8
195	20120615084331	146.4	−3.4	11	−0.63	0.59	0.04	0.29	−0.79	1.12	17	5.3	93.5
196	20120707033527	153.2	−4.8	55	3.99	0.73	−4.72	−2.02	−0.84	0.14	17	5.7	91.3
197	20120722070212	149.8	−4.8	3	−0.86	3.05	−2.18	2.02	−2.01	0.67	17	5.6	92
198	20120728200356	153.2	−4.8	51	5.07	−5.19	0.12	4.11	2.24	0.73	18	6.5	82.2
199	20120801204339	144.8	−4.4	39	0.61	−1.34	0.73	−0.47	0.87	0.28	17	5.4	99.9
200	20120802095641	153.2	−5.0	51	1.29	−1.29	0.00	0.95	0.56	0.05	18	6.1	82.1
201	20120927235348	157.4	−9.0	7	3.50	−0.90	−2.60	1.17	−3.30	1.41	17	5.7	93.8
202	20120928232231	157.6	−9.2	3	0.15	−0.02	−0.13	0.55	−1.12	0.22	17	5.2	79.5
203	20121106142035	149.0	−3.6	15	−0.14	1.07	−0.93	0.64	−0.70	1.41	17	5.4	75.4
204	20121114234155	151.8	−6.0	11	2.02	−1.59	−0.43	0.79	0.62	−0.61	17	5.5	83.2
205	20121115082148	148.4	−3.4	11	−1.44	6.15	−4.71	0.48	−3.38	5.64	17	5.8	99.9
206	20121119094434	151.8	−6.0	15	−9.46	4.54	4.91	−1.86	−6.96	5.05	17	5.9	91.4
207	20121129111021	145.6	−3.4	11	−0.60	0.17	0.44	0.46	−1.02	1.08	18	6.0	74
208	20130201021722	147.8	−7.0	3	−1.31	−3.94	5.25	4.72	6.54	1.48	17	5.9	60.8
209	20130302214722	145.2	−3.4	3	0.21	−0.19	−0.02	0.09	−1.24	1.10	17	5.3	91.9
210	20130305060634	152.6	−5.4	15	2.63	−2.90	0.27	3.51	0.47	−0.73	17	5.7	82.6
211	20130310164918	151.6	−5.6	59	3.64	−3.52	−0.12	0.58	−0.46	−1.10	17	5.7	94.8
212	20130310225151	148.4	−6.8	15	−0.10	−1.24	1.34	1.20	−0.83	6.22	18	6.4	93.4
213	20130414013222	154.6	−6.8	23	5.51	−2.89	−2.62	3.53	−1.77	2.39	18	6.4	85.4
214	20130416100023	154.4	−6.8	23	3.39	−0.44	−2.95	0.80	−2.64	0.96	17	5.7	94.6
215	20130416225526	142.6	−3.2	15	4.63	−1.97	−2.66	1.07	2.79	4.82	18	6.4	79.3
216	20130420034201	152.2	−5.2	43	2.99	−2.67	−0.32	1.03	0.15	−0.83	17	5.6	95.5
217	20130423231442	152.2	−4.0	7	−2.43	7.83	−5.40	−2.51	−3.28	0.15	18	6.5	79.9
218	20130619065237	151.2	−3.8	3	−0.73	1.90	−1.16	−1.47	−1.53	0.29	17	5.5	89.3
219	20130624080139	148.8	−6.8	31	2.27	−2.79	0.52	1.98	−0.40	0.01	17	5.6	72.9
220	20130624095543	148.8	−6.8	15	2.33	−2.29	−0.04	1.45	0.05	−0.13	17	5.5	97.3
221	20130704171560	155.6	−7.4	39	1.24	−0.82	−0.42	−0.08	−0.22	0.75	18	6.0	84.1
222	20130710171646	149.0	−5.0	3	−0.48	0.89	−0.40	0.92	−0.30	1.38	17	5.4	81.6
223	20130716093554	154.6	−6.6	39	7.95	−4.24	−3.71	1.25	0.80	4.10	17	5.9	97
224	20130902043016	154.8	−7.0	39	8.74	−4.41	−4.33	0.66	0.29	4.51	17	5.9	98
225	20130918205330	144.2	−3.4	3	0.24	−0.07	−0.16	0.19	−1.06	2.06	17	5.4	73.9
226	20131016103058	154.8	−6.8	39	1.38	−0.71	−0.67	0.09	0.14	0.79	19	6.7	88.4
227	20140125170004	155.8	−8.2	23	0.92	0.40	−1.32	0.75	−0.28	0.94	17	5.4	61.9
228	20140209145639	154.2	−6.2	39	8.36	−3.75	−4.60	0.05	1.50	4.41	17	5.9	97.3
229	20140311220309	148.6	−3.6	19	−0.10	1.32	−1.22	−0.25	−0.53	1.26	18	6.1	89.2
230	20140320184413	152.8	−5.4	15	1.32	−1.27	−0.05	1.89	0.05	−0.39	17	5.5	99.5
231	20140320184413	152.8	−5.4	15	1.29	−1.24	−0.04	1.97	0.04	−0.39	17	5.5	99.6
232	20140320211509	152.8	−5.6	27	3.08	−3.08	0.00	3.03	0.34	−0.70	17	5.7	94.1
233	20140331134057	147.2	−8.4	3	−0.95	0.87	0.08	−3.65	4.01	−1.91	17	5.7	56.7
234	20140405033436	142.0	−3.6	23	−0.74	−4.89	5.63	2.40	−2.67	3.32	16	5.1	93.9
235	20140411125516	154.8	−7.2	19	2.02	−0.96	−1.06	1.03	−1.14	0.96	17	5.5	96.3
236	20140411143342	155.0	−6.8	39	−1.67	1.11	0.55	0.71	−3.38	0.26	17	5.6	43.6
237	20140411081645	155.0	−7.2	19	3.64	−2.33	−1.32	2.17	−1.53	1.50	18	6.3	89.5
238	20140411070723	155.0	−7.0	39	4.03	−2.20	−1.83	−0.18	−0.12	1.91	19	7.0	94.6
239	20140412155926	155.0	−7.6	3	2.76	−1.66	−1.10	9.00	−7.27	1.18	17	5.9	97.2
240	20140412052423	155.2	−7.4	11	1.00	−0.82	−0.18	0.73	−0.48	0.37	18	6.0	97.3
241	20140419010403	155.0	−7.0	35	7.77	−5.25	−2.52	1.87	−1.50	3.64	18	6.5	99.9
242	20140419132760	154.6	−7.2	31	1.26	−0.68	−0.58	0.48	−0.31	0.65	20	7.3	97.4
243	20140420041730	154.6	−7.2	15	2.50	−1.92	−0.59	2.62	−1.64	0.97	17	5.6	95.8
244	20140420001558	155.4	−7.2	15	1.57	−0.97	−0.60	0.62	−0.59	0.64	18	6.1	86.5

Table 1. (continued)

Number	Origin Time	Longitude	Latitude	Depth	Mrr	Mtt	Mff	Mrt	Mrf	Mtf	Exp	M_w	DC%
245	20140507042033	154.8	−7.0	3	1.26	−8.77	7.51	4.34	4.35	0.86	17	5.9	95.1
246	20140704150027	152.8	−6.4	15	−5.05	3.73	1.32	−2.10	0.70	0.24	18	6.4	50.1
247	20140713200035	151.2	−4.4	3	−2.33	7.22	−4.89	−8.61	−8.02	0.50	17	6.0	95.9
248	20140715094457	151.4	−4.6	7	−1.28	4.19	−2.91	−1.81	−3.04	1.04	17	5.7	98.8
249	20140715103029	151.4	−4.6	15	−0.46	3.38	−2.92	−0.93	−2.51	1.55	17	5.7	86.9
250	20140715163900	151.4	−4.6	7	−1.40	4.01	−2.60	−2.22	−3.25	1.12	17	5.7	96.2
251	20140729132740	146.6	−3.4	15	−0.36	−0.17	0.53	0.47	−1.16	1.14	18	6.0	77.3
252	20140730160058	155.0	−7.6	3	0.47	−0.32	−0.15	1.87	−0.79	0.15	18	6.1	93.5
253	20140803044848	146.6	−3.2	23	−2.05	−0.55	2.60	1.47	−7.32	5.62	16	5.2	93.6
254	20140813055436	145.4	−3.2	3	−0.33	−0.01	0.34	6.24	−8.43	1.98	17	5.9	65.4
255	20140821021131	150.6	−5.2	7	−2.59	9.22	−6.63	−1.62	−4.52	3.06	17	5.9	89
256	20140822173924	154.4	−7.6	3	−3.36	4.27	−0.91	−6.03	8.15	−3.30	16	5.2	83.6
257	20140822142949	147.0	−6.8	3	1.41	−0.60	−0.81	1.07	−3.68	1.36	17	5.6	91
258	20140925091350	156.4	−9.4	7	−0.20	0.25	−0.05	0.01	−0.14	1.32	18	5.9	73
259	20140930192348	153.2	−4.2	19	3.53	3.59	−7.12	−3.70	−2.55	3.73	16	5.2	98.3
260	20141019185832	150.8	−3.2	11	−1.50	3.12	−1.61	1.27	−3.02	6.97	16	5.1	99.5
261	20141107033355	148.4	−6.4	39	8.63	−8.32	−0.31	1.58	−0.25	0.28	18	6.6	93.1
262	20141207012202	154.4	−6.6	7	3.56	−0.87	−2.69	3.29	−4.69	1.71	18	6.4	96
263	20141209023331	154.4	−6.4	15	1.07	−0.66	−0.41	−0.70	0.32	0.34	17	5.3	72.9
264	20150213170204	148.8	−3.4	23	−0.88	1.11	−0.23	0.55	−1.11	1.52	17	5.4	83.5
265	20150307221856	151.8	−6.6	39	2.36	−0.56	−1.80	−1.29	0.54	−1.70	17	5.6	92.6
266	20150329234831	152.8	−5.4	31	1.14	−1.06	−0.07	0.92	0.07	−0.26	20	7.3	97.1
267	20150331121824	152.4	−5.0	43	9.34	−9.09	−0.25	4.02	0.43	−1.87	17	5.9	97.9
268	20150403192224	153.2	−5.2	27	3.34	0.85	−4.19	1.99	0.66	−1.61	16	5.0	83.6
269	20150403192224	153.0	−5.6	23	3.58	0.41	−3.98	1.88	0.62	−1.99	16	5.0	80.4
270	20150403211754	147.8	−6.4	35	8.27	−6.96	−1.31	2.06	−0.54	2.09	17	5.9	85.4
271	20150415102206	151.4	−3.6	7	−0.62	1.28	−0.66	0.19	−0.90	1.12	17	5.4	97.3
272	20150421112108	150.0	−6.4	39	1.58	−1.59	0.01	0.40	0.18	−0.20	17	5.4	97.5
273	20150430104502	151.8	−5.6	35	9.00	−7.39	−1.61	2.21	1.36	−3.12	18	6.6	94.4
274	20150501080603	151.8	−5.6	47	1.65	−1.47	−0.18	0.20	−0.11	−0.50	19	6.7	97.2
275	20150503234055	151.8	−5.6	31	4.97	−4.57	−0.40	2.69	0.55	−1.27	17	5.8	98.4
276	20150503234056	151.8	−5.6	31	4.88	−4.56	−0.32	2.69	0.52	−1.38	17	5.7	97.3
277	20150503223239	151.8	−5.8	19	5.68	−5.65	−0.04	5.53	−0.10	−1.57	17	5.8	96.3
278	20150505081657	152.2	−6.0	7	2.71	−2.25	−0.46	2.27	0.77	−0.95	17	5.6	97.1
279	20150505014406	152.2	−5.4	31	7.88	−6.61	−1.27	1.98	1.06	−3.23	19	7.2	94
280	20150506031709	152.6	−6.0	3	0.95	−0.29	−0.65	2.26	−0.93	0.11	17	5.5	63.2
281	20150507113259	154.4	−7.2	3	−6.09	5.00	1.09	5.42	0.46	−2.28	16	5.2	83.5
282	20150507071019	154.6	−7.4	3	−2.04	1.58	0.46	−2.42	1.83	−0.90	19	6.9	99.3
283	20150508090704	152.6	−5.8	11	2.17	−1.84	−0.34	1.67	0.57	−0.31	16	4.9	79.7
284	20150508075206	150.0	−6.4	39	7.82	−7.96	0.14	1.84	0.83	−1.04	17	5.9	94.6
285	20150518170452	154.4	−7.4	3	−1.88	1.33	0.56	−4.19	3.77	−0.97	17	5.7	97.6
286	20150523192817	152.6	−5.0	35	5.37	−4.80	−0.58	4.66	0.91	−1.62	17	5.8	98
287	20150610154646	151.8	−4.2	3	−2.21	6.43	−4.22	−1.77	2.58	0.41	16	5.1	80.8
288	20150613070858	143.8	−3.2	3	1.03	−0.68	−0.34	2.45	−1.72	0.49	17	5.5	99.8
289	20150627122402	153.4	−5.4	7	3.15	0.25	−3.40	−1.33	−0.14	−0.86	16	5.0	97
290	20150630033929	151.6	−5.8	43	1.00	−1.01	0.00	0.17	−0.08	−0.29	18	5.9	87.5
291	20150710041242	158.4	−9.6	3	0.14	−0.28	0.14	−0.59	−0.16	1.05	19	6.6	99.9
292	20150810042431	157.8	−9.4	11	0.47	1.07	−1.54	−2.06	−0.75	7.52	17	5.8	99.3
293	20150810041215	158.2	−9.4	7	1.73	0.92	−2.65	−1.65	−1.61	8.18	18	6.5	79.9
294	20150812184924	157.8	−9.4	7	0.67	1.08	−1.75	−1.16	−1.23	5.93	18	6.4	94.5
295	20150816210509	154.0	−6.0	43	4.08	−1.39	−2.68	1.28	−3.07	2.28	16	5.0	92
296	20150912221607	147.4	−6.4	31	1.89	−1.81	−0.08	0.11	−0.01	0.47	17	5.5	95.7
297	20150916140322	151.6	−6.4	11	−1.04	0.70	0.34	−0.66	−0.51	0.24	18	6.0	66.7
298	20151104070631	149.6	−3.6	7	−1.75	6.46	−4.71	0.07	−2.51	3.15	16	5.1	84
299	20151104054310	149.8	−3.6	11	−1.95	5.73	−3.78	3.81	−2.69	3.95	16	5.2	97.9
300	20151104055227	149.6	−3.6	7	−0.89	1.84	−0.94	1.01	−1.11	1.47	17	5.5	87.9
301	20151105163237	150.6	−3.6	15	−0.53	1.43	−0.90	−0.04	−0.83	0.74	17	5.4	98.5
302	20151118183104	158.2	−9.6	23	1.44	−0.44	−1.00	0.12	−1.71	1.03	19	6.8	99.8
303	20151229015140	154.6	−6.6	31	3.43	−0.96	−2.48	−3.53	1.59	1.99	17	5.7	92.7
304	20160126031020	153.2	−5.4	19	−1.10	−0.27	1.37	0.55	0.06	0.14	18	6.0	98.7
305	20160130120246	147.0	−3.4	15	−0.56	0.75	−0.19	0.47	−1.18	1.82	17	5.4	83.1

Table 1. (continued)

Number	Origin Time	Longitude	Latitude	Depth	Mrr	Mtt	Mff	Mrt	Mrf	Mtf	Exp	M_w	DC%
306	20160131025004	147.0	−3.0	7	2.87	−2.55	−0.32	1.08	0.33	−0.58	17	5.6	88.1
307	20160208161912	154.6	−6.8	39	5.05	−1.98	−3.07	0.84	−2.24	1.60	18	6.4	68.6
308	20160303215759	148.6	−3.4	19	−1.54	1.78	−0.24	0.17	−1.37	1.53	17	5.5	97.5
309	20160318003124	153.0	−5.0	43	0.52	2.11	−2.64	−0.41	−0.94	−0.57	17	5.5	50.3
310	20160328035659	151.2	−4.4	7	−0.46	1.12	−0.66	−0.70	−0.69	−0.04	17	5.3	93.2
311	20160401192455	144.8	−3.4	15	−0.59	0.10	0.49	0.89	−0.82	2.07	18	6.1	87.7
312	20160409084235	147.8	−6.0	27	−1.80	−3.90	5.70	0.45	−0.48	3.10	16	5.1	48.4
313	20160410042159	151.2	−4.6	7	−3.40	6.26	−2.85	−5.84	−5.96	0.79	16	5.2	98.6
314	20160420104155	153.2	−5.6	19	1.71	−2.07	0.35	3.56	−0.02	0.04	16	4.9	83.2
315	20160421142811	142.8	−3.8	35	−5.90	−1.66	7.56	−4.50	−0.64	3.45	16	5.2	96.7
316	20160527150341	152.2	−5.2	39	5.09	−4.50	−0.59	0.79	2.62	−2.60	16	5.1	99.7
317	20160725195001	151.2	−4.2	3	−0.64	1.67	−1.03	−2.20	−2.48	0.29	17	5.6	96.2
318	20160726063128	151.4	−3.6	7	−4.26	8.05	−3.79	0.54	−4.27	2.00	16	5.2	97.4

[a]Events #1 and #2 described in section 4 are highlighted.

In this study, we have considered events with DC <70% in the GCMT catalogue as "low DC sources," which makes a set of 78 events spread across the study region (they are not restricted to a specific location, depth, or time interval; Figure 10). Our CSCMT-3D solutions show a significant increase in DC% compared to that of the GCMT for 70 events. In total, our CSCMT-3D solutions show DC% >80 for 65% of the GCMT's low DC events. Another example of a significant improvement of DC% is the event 22 August 2014 14:29:50 (Figure 10) with 68% increase in DC.

We observe some exceptions. A severe case is an event that occurred on 25 September 2006 07:46:30 with M_w 5.4 (Figure 10), where the CSCMT-3D solution shows only 4% DC (GCMT reported 32% DC). This is the only event in our CSCMT-3D catalogue with DC% <40. This earthquake is an excellent candidate to be investigated as potentially being the consequence of a complex tectonic event, which is beyond the scope of this study.

4.2. Shallow Crustal Events; Event 2: 10 August 2009 17:46:23

From our third synthetic test (Figure 8) we concluded that, using AMSAN19, the pure vertical dip-slip mechanisms produce similar ground motions (but still nonzero amplitude) for the depth interval 3–19 km; hence, there is little depth resolution. However, the rest of the elementary bases are recovered well for a source at 7 km depth using our station distribution. For a vertical dip-slip mechanism, CSCMT-3D still provides a reasonable recovery of the location and MT components, which allows us to perform CSCMT-3D inversions for shallow crustal sources.

The event that occurred on 10 August 2009 17:46:23 has been reported with a depth of 12.0 km in the GCMT catalogue (marked as fixed depth in the catalogue) and 30.5 km in the ISC catalogue. Using 12 stations (Figure 11), the CSCMT-3D solution for this event reveals 95% DC and a thrust mechanism. The location is marked by a distinct peak of variance reduction at 7 km depth (variance reduction reaches 0.71 at the optimum location and time). The estimated DC of 95% represents a 25% increase in comparison to the GCMT solution. Both CSCMT-3D and GCMT estimate M_w 5.7.

In our CSCMT-1D, the variance reduction in the depth range of 3–19 km varies a little (between 0.34 and 0.37), which then gradually drops to zero at 30 km depth. The constraint on horizontal location is even worse, and the optimum location is at the western edge of the numerical grid at 11 km depth (Figure 11a). The CSCMT-1D has M_w 5.6, a DC of 62%, and a reverse mechanism similar to the GCMT.

For most of the stations, the ak135 Earth model provides an acceptable variance reduction of 0.3 (note that the AMSAN19 synthetics provide significantly improved variance reduction) except for the station KAPI, where there is a significant mismatch between synthetics and real data with negative variance reduction (as low as −0.76 for BHN component). The AMSAN19 synthetics fit the data of station KAPI (the BHN component has variance reduction of 0.51) as well as other stations (Figure 11c).

About 30% of the events in this study have depth of 12 km in the GCMT catalogue. Our CSCMT-3D solutions show centroid depths of 3–23 km for these events (Figure 12).

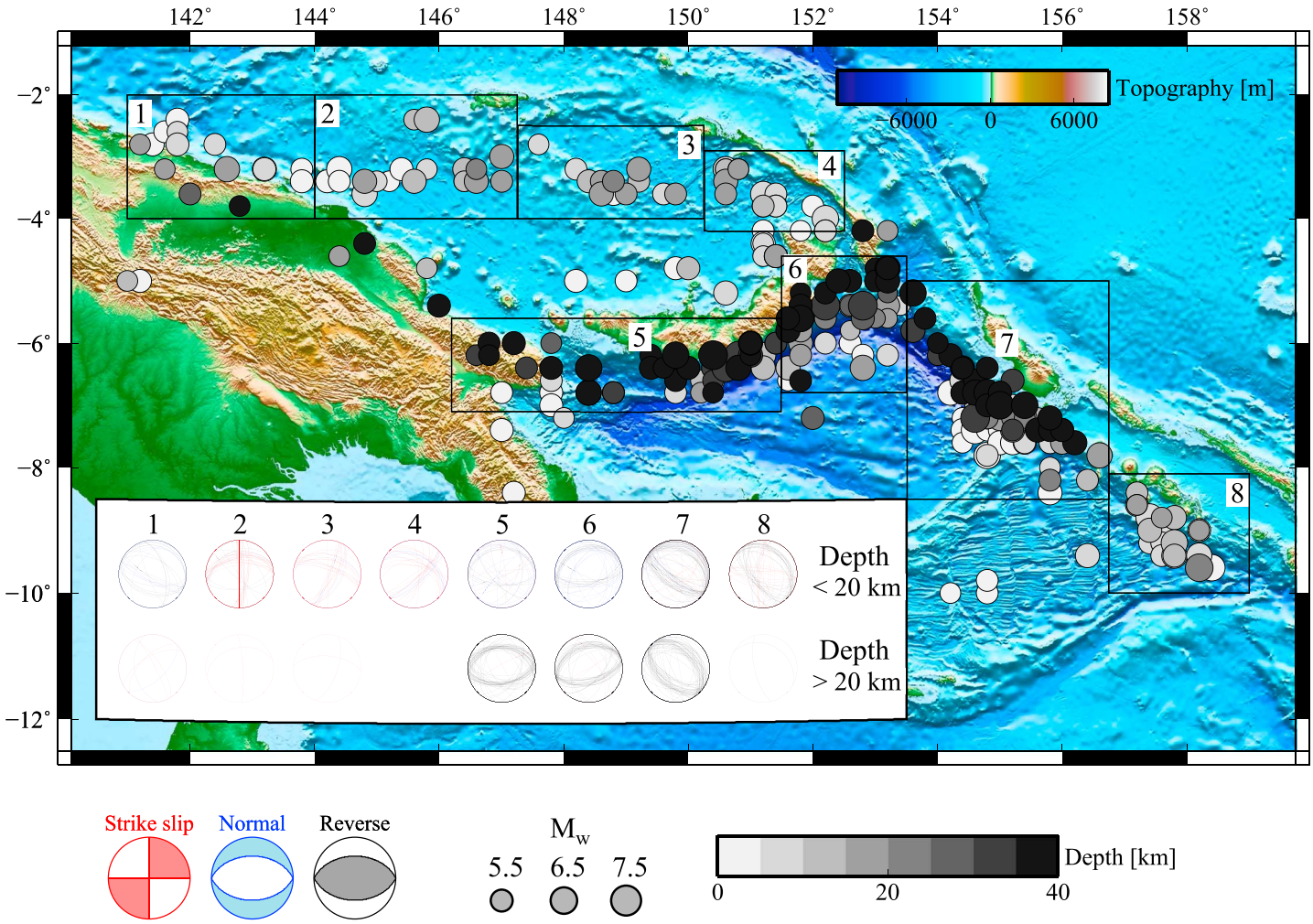

Figure 16. Summary map of all 318 earthquakes analyzed in this study. Earthquakes are plotted at the newly obtained centroid locations with circles colored for centroid depth. The size is proportional to the moment magnitudes in our CSCMT-3D catalogue. The seismicity is divided into eight subregions, numbered 1 to 8, where regions 1 to 4 cover the Bismarck Sea Seismic Lineation as well as the New Guinea Trench (Figure 13), whereas regions 5 to 8 cover the Papua New Guinea and Solomon Islands subduction. The nodal planes of mechanisms in each subregion are plotted for two depth intervals, shallower and deeper than 20 km. These nodal planes are colored such that the strike-slip mechanisms are red, normal are blue, and reverse are black.

4.3. Improving Tectonic Interpretations: Example From 37 Events North of Papua New Guinea

Events 1 and 2 showed the impact of 3-D heterogeneity on CMT solutions that we expected already according to our synthetic tests. Event 1 clearly demonstrates that even in the presence of a poor azimuthal coverage the 3-D heterogeneous Earth model provides a distinct peak of variance reduction for depth and horizontal location of the centroid.

To show how the 3-D heterogeneity can affect the tectonic interpretations, we selected 37 events that occurred around two known tectonic settings north of Papua New Guinea (PNG) where the western edge of the BSSL [*Llanes et al.*, 2009] meets the New Guinea Trench [*Koulali et al.*, 2015] (Figure 13a). In comparison with ak135, AMSAN19 increased the fit to the data by ~40% (Figure 13b).

Consequently, depths and lateral locations are identified by a distinct peak of high variance reduction, while ak135 produces a diffuse pattern with no clear peak for all 37 events. This is quite visible when we compare the locations of CSMCT-3D and CSMCT-1D (Figures 13c, 13d, and 13e). The CSCMT-1D displays such that no clear pattern can be observed for the well-known BSSL [*Llanes et al.*, 2009], but the CSCMT-3D reveals a similar pattern to the GCMT and to the geological evidence like high-resolution bathymetry data from *Llanes et al.* [2009] (Figure 13). This is a significant improvement, and it argues for of using continental 3-D

heterogeneous Earth models to improve CMT solutions wherever these models and a good azimuthal coverage are present. Moreover, as seen in the cross section XX′ (Figure 13), the CSCMT-3D centroids display a reasonable pattern for a subducting plate down to the depth of 30 km while the CSCMT-1D centroids are distributed in a much wider depth range of 7–50 km. An interesting observation is that the CSCMT-1D catalogue has similar mechanisms to those of GCMT, but with a strong scatter in centroid location and time and generally lower DC%.

5. Discussions and Conclusions

The increase in DC% of the MT was significant when we used the 3-D Earth model AMSAN19 in comparison with the 1-D Earth model ak135 for 37 events north of PNG. This increase in DC% as documented by our synthetic tests (section 3) and the examples from the observed earthquake data (Figures 9–11, and 13) is a result of the inclusion of the 3-D heterogeneity effects.

About 81% of the events (258 out of 318) have DC >80% in the CSCMT-3D catalogue, whereas this is the case for only 58% (186 out of 318) in the GCMT catalogue (Figure 14a). Leaving out the exceptional event on 25 September 2006 08:46:30, mentioned above, and comparing the DC% for each event reveals several interesting points. While the GCMT catalogue displays a wide range of DC percentages, from ~10 to 99, we observe DC >60% for 307 of them (white circles in Figure 14b), which indicates a significantly less scattered DC%. Second, there are only 11 events with DC% <60 in the CSCMT-3D catalogue, where two of them show an increase in DC% compared to GCMT (light gray circles in Figure 14b). The remaining nine events marked with black and dark gray circles in Figure 14b constitute only 3% of the entire data set.

The 3-D heterogeneity is not the only parameter affecting the DC%. One plausible reason for spurious DC components is a higher noise level on teleseismic records used in the GCMT inversion, particularly for the events with $M_w < 5.5$. The difference in DC% of the two data sets with respect to moment magnitude shows a higher discrepancy for smaller events (Figure 15a). Another possible reason affecting the discrepancy in DC component percent between the two catalogues is the different depth to the centroids. Our solutions reveal shallower depths for the events which are fixed to 12.0 km in the GCMT catalogue (Figure 15b). The difference in DC% is relatively higher for all shallow events and relatively lower for deeper events, where the agreement between the centroid depth of CSCMT-3D and GCMT catalogue increases (Figure 15b).

The only parameter in our CSCMT-3D solutions that remains relatively similar to that of GCMT catalogue is the moment magnitude (Figure 15a). The CSCMT-1D displays lower moment magnitudes in most cases, which is due to the relatively lower amplitude of the synthetics. The non-DC part of the MT is not the only component that is affected by the 3-D heterogeneity. For example, event 2 (line 112 in Table 1; also described in section 4.2) and several other events shown in Figures 11 and 13 have different strike, dip, and rake angles compared to those of the GCMT. To make a comparison between MT components in the CSCMT-3D and GCMT catalogues more complete, we calculated the angle ω_{9D} as described in section 2.1 for all 318 earthquakes. The maximum discrepancy between MT components of CSCMT-3D and GCMT (up to $\omega_{9D} = 100°$) occurs for shallow depths of 3–11 km and moment magnitude <6.0. We infer that depth and magnitude are the two main parameters that seem to control the differences in MT components. At shallow depths (<30 km) and for events with $M_w < 5.5$, we observed a significant difference in MT components between CSCMT-3D and GCMT catalogues. We infer that these differences as well as DC percentage are mainly due to neglecting the 3-D heterogeneity of the Earth, elevated noise levels on teleseismic distant stations, significant contribution of information from surface waves for small events, and the shallowest possible depth limit of 12 km in the GCMT catalogue.

The CSCMT-3D catalogue reveals a significant improvement in comparison with the CSCMT-1D solutions for a selected subset of 37 events at the junction of the BSSL and the New Guinea Trench. While the scatter in CSCMT-1D locations is significant, the CSCMT-3D solutions followed the well-known seismic line with documented bathymetry lineaments [*Llanes et al.*, 2009]. The depths reported in CSCMT-3D show significant improvement; e.g., the New Guinea Trench can be observed as a shallow subduction down to the depth range of 25–30 km [*Tregoning and Gorbatov*, 2004].

This proves the capability of using a 3-D velocity model at continental scale to improve the depth and location recovery for shallow events, which increases the chance for better tectonic interpretations and hazard assessments.

The CSCMT-3D catalogue has the potential to bring new insights into tectonic interpretations of the region (Figure 16). The overall centroid locations follow the observable surface tectonic features. The centroid depths show shallow seismicity at the BSSL, but a gradual increase in depth along the subduction at the New Guinea trench and Solomon Islands (note the darker colors for deeper earthquakes in Figure 16).

To illustrate the mechanisms, we divide the catalogue into eight subregions, numbered 1 to 8, and in each subregion, we plot the nodal planes on top of each other, with color codes of red for strike slip, black for reverse and blue for normal. The first four cover the New Guinea Trench and BSSL. With only two events deeper than 20 km, most of the seismicity along BSSL is within the top 20 km, where the strike-slip mechanisms on north and north-east dipping plates are dominant. At the New Guinea Trench, except few events with normal mechanism, the rest are thrust faults dipping south-west.

Subregions 5 to 8 cover four segments of the highly active megathrust subduction along the New Guinea Trench and Solomon Islands (Figure 16). Here the seismicity extends deeper along the subducting plate. An interesting common feature is the low dip angle of the thrust faults for events shallower than 20 km, while the strike of the dipping plate changes from north at region 5 to north-west at region 6 and north-east at regions 7 and 8. At regions 5, 6, and 7 the deeper events with reverse mechanism have higher dip angle of ~45°, indicating that the subducting plate becomes steeper as it subducts. Region 8 that encompasses Solomon Islands seems to have significantly lower seismicity below depth 20 km with only a single earthquake.

We have not yet started utilizing structural 3-D models on the global scale for a determination of source parameters. However, with increasing computational power and quality of seismic data sets, we should soon move to this mode. The results presented here strongly argue that this is an inevitable direction forward in our pursuit to better understand earthquake generation and its relationship with tectonics.

Acknowledgments
This research was fully funded by the Australian Research Council Discovery Proposal DP140102533. Calculations were performed on the ANU Terrawulf cluster, a computational facility developed with support from the AuScope initiative. AuScope Ltd. is funded under the National Collaborative Research Infrastructure Strategy (NCRIS), an Australian Commonwealth Government Programme. This research/project was undertaken with the assistance of resources and services from the National Computational Infrastructure (NCI), which is supported by the Australian government. The facilities of IRIS Data Services, and specifically the IRIS Data Management Center, were used for access to waveform and metadata required in this study. The IRIS DS is funded through the National Science Foundation and specifically the GEO Directorate through the Instrumentation and Facilities Program of the National Science Foundation under cooperative agreement EAR-0004370. The seismic networks whose data we used in this study are IRIS/IDA with network code II and DOI number 10.7914/SN/II, Global Seismograph Network with network code IU and DOI number 10.7914/SN/IU, GEOSCOPE with network code G and DOI number 10.18715/GEOSCOPE.G, and Australian National Seismograph Network (ANSN), with network code AU operated by Geoscience Australia. The authors would like to thank the two anonymous reviewers for their valuable comments.

References

Adamová, P., E. Sokos, and J. Zahradník (2009), Problematic non-double-couple mechanism of the Amfilochia M_w 5 earthquake, western Greece, *J. Seismol.*, *13*, 1–12.
Backus, G., and M. Mulcahy (1976), Moment tensors and other phenomenological descriptions of seismic sources—Continuous displacements, *Geophys. J. R. Astron. Soc.*, *46*, 341–361.
Bouchon, M. (1976), Teleseismic body wave radiation from a seismic source in layered medium, *Geophys. J. R. Astron. Soc.*, *47*, 515–530.
Burridge, R., and L. Knopoff (1964), Body force equivalents for seismic dislocations, *Bull. Seismol. Soc. Am.*, *54*, 1875–1888.
Červený, V. (2001), *Seismic Ray Theory*, pp. 91–93, Cambridge Univ. Press, Cambridge.
Chapman, C. (1994), Reflection/transmission coefficient reciprocities in anisotropic media, *Geophys. J. Int.*, *116*, 498–501.
Chen, P., L. Zhao, and T. H. Jordan (2007), Full 3D tomography for crustal structure of the Los Angeles region, *Bull. Seismol. Soc. Am.*, *97*, 1094–1120.
Claerbout, J. (1976), *Fundamentals of Geophysical Data Processing*, pp. 174–178, Mc-Graw-Hill, New York.
Davies, H. L., J. Lock, D. L. Tiffin, E. Honza, Y. Okuda, F. Murakami, and K. Kisimoto (1987), Convergent tectonics in the Huon Peninsula region, Papua New Guinea, *Geo-Mar. Lett.*, *7*, 143–152.
de Hoop, M., and A. de Hoop (2000), Wave-field reciprocity and optimalization in remote sensing, *Proc. R. Soc. London, Ser. A*, *456*, 641–682.
Dreger, D., H. Tkalčić, and M. Johnston (2000), Dilatational processes accompanying earthquakes in the Long Valley Caldera, *Science*, *288*, 122–125.
Dziewonski, A. M., T.-A. Chou, and J. H. Woodhouse (1981), Determination of earthquake source parameters from waveform data for studies of global and regional seismicity, *J. Geophys. Res.*, *86*, 2825–2852, doi:10.1029/JB086iB04p02825.
Eisner, L., and W. Clayton (2001), A reciprocity method for multiple-source simulations, *Bull. Seismol. Soc. Am.*, *91*(3), 553–560.
Eisner, L., and W. Clayton (2005), Simulating strong ground motion from complex sources by reciprocal Green's functions, *Stud. Geophys. Geod.*, *49*(3), 323–342.
Fichtner, A., and H. Tkalčić (2010), Insights into the kinematics of a volcanic caldera drop: Probabilistic finite-source inversion of the 1996 Bardarbunga, Iceland, earthquake, *Earth Planet. Sci. Lett.*, *297*(3–4), 607–615.
Fichtner, A., H. Igel, H. Bunge, and B. L. N. Kennett (2009a), Simulation and inversion of seismic wave propagation on continental scales based on a spectral-element method, *J. Numerical Anal., Industrial Appl. Math.*, *4*, 11–22.
Fichtner, A., B. L. N. Kennett, H. Igel, and H.-P. Bunge (2009b), Full seismic waveform tomography for upper-mantle structure in the Australasian region using adjoint methods, *Geophys. J. Int.*, *179*, 1703–1725.
Fichtner, A., B. L. N. Kennett, H. Igel, and H.-P. Bunge (2010), Full waveform tomography for radially anisotropic structure: New insight into present and past states of the Australasian upper mantle, *Earth Planet. Sci. Lett.*, *290*, 270–280.
Frohlich, C., and S. D. Davis (1999), How well constrained are well-constrained *T*, *B*, and *P* axes in moment tensor catalogs?, *J. Geophys. Res.*, *104*, 4901–4910, doi:10.1029/1998JB900071.
Gallovič, F., M. Kaser, J. Burjanek, and C. Papaioannou (2010), Three-dimensional modeling of near-fault ground motions with nonplanar rupture models and topography: Case of the 2004 Parkfield earthquake, *J. Geophys. Res.*, *115*, B03308, doi:10.1029/2008JB00617.

Graves, R. W., and R. Clayton (1992), Modeling path effects in 3-dimensional basin structures, *Bull. Seismol. Soc. Am.*, *82*, 81–103.
Graves, R., and D. Wald (2001), Resolution analysis of finite fault source inversion using 1D and 3D Green's functions. I. Strong motions, *J. Geophys. Res.*, *106*, 8745–8766, doi:10.1029/2000JB900436.
Hill, K. C., and R. Hall (2003), Mesozoic-Cenozoic evolution of Australia's New Guinea margin in a west Pacific context, *Geol. Soc. Am. Spec. Pap.*, *372*, 265–290.
Hingee, M., H. Tkalčić, A. Fichtner, and M. Sambridge (2012), Seismic moment tensor inversion using a 3-D structural model: Applications for the Australian region, *Geophys. J. Int.*, *184*, 949–964.
Hjörleifsdóttir, V., and G. Ekström (2010), Effects of three-dimensional Earth structure on CMT earthquake parameters, *Phys. Earth Planet. Inter.*, *179*, 178–190.
Johnson, T., and P. Molnar (1972), Focal mechanisms and plate tectonics of the southwest Pacific, *J. Geophys. Res.*, *77*, 5000–5032, doi:10.1029/JB077i026p05000.
Kennett, B. L. N., E. R. Engdahl, and R. Buland (1995), Constraints on seismic velocities in the Earth from travel times, *Geophys. J. Int.*, *122*, 108–124.
Kikuchi, M., and H. Kanamori (1991), Inversion of complex body waves—III, *Bull. Seismol. Soc. Am.*, *81*, 2335–2350.
Kim, Y., Q. Liu, and J. Tromp (2011), Adjoint centroid-moment tensor inversions, *Geophys. J. Int.*, *186*(1), 264–278.
Komatitsch, D., and J. Tromp (1999), Introduction to the spectral-element method for 3-D seismic wave propagation, *Geophys. J. Int.*, *139*(3), 806–822.
Koulali, A., P. Tregoning, S. McClusky, R. Stanaway, L. Wallace, and G. Lister (2015), New insights into the present-day kinematics of the central and western Papua New Guinea from GPS, *Geophys. J. Int.*, *202*, 993–1004.
Kühn, D., and V. Vavryčuk (2013), Determination of full moment tensors of microseismic events in a very heterogeneous mining environment, *Tectonophysics*, *589*, 33–43.
Lee, E. J., P. Chen, T. H. Jordan, and L. Wang (2011), Rapid full-wave centroid moment tensor (CMT) inversion in a three-dimensional Earth structure model for earthquakes in Southern California, *Geophys. J. Int.*, *186*(1), 311–330.
Liu, Q., J. Polet, D. Komatisch, and J. Tromp (2004), Spectral-element moment tensor inversions for earthquakes in Southern California, *Bull. Seismol. Soc. Am.*, *94*, 1748–1761.
Llanes, P., E. Silver, S. Day, and G. Hoffman (2009), Interactions between a transform fault and arc volcanism in the Bismarck Sea, Papua New Guinea, *Geochem. Geophys. Geosyst.*, *10*, Q06013, doi:10.1029/2009GC002430.
Magistrale, H., S. Day, R. Clayton, and R. Graves (2000), The SCEC Southern California reference 3D seismic velocity model version 2, *Bull. Seismol. Soc. Am.*, *90*, 65–76.
Mustać, M., and H. Tkalčić (2016), Point source moment tensor inversion through a Bayesian hierarchical model, *Geophys. J. Int.*, *204*(1), 311–323.
Okamoto, R. (2002), Full waveform moment tensor inversion by reciprocal finite difference Green's function, *Earth Planets Space*, *54*, 715–720.
Serpetsidaki, A., E. Sokos, G.-A. Tselentis, and J. Zahradnik (2010), Seismic sequence near Zakynthos Island, Greece, April 2006: Identification of the activated fault plane, *Tectonophysics*, *480*, 23–32.
Shearer, P. (1999), *Introduction to Seismology*, pp. 241–297, Cambridge Univ. Press, Cambridge.
Sokos, E., J. Zahradník, A. Kiratzi, J. Janský, F. Gallovič, O. Novotný, J. Kostelecký, A. Serpetsidaki, and G.-A. Tselentis (2012), The January 2010 Efpalio earthquake sequence in the western Corinth Gulf (Greece), *Tectonophysics*, *530*(531), 299–309.
Somerville, P., K. Irikura, R. Graves, S. Sawada, D. Wald, N. Abrahamson, Y. Iwasaki, T. Kagawa, N. Smith, and A. Kowada (1999), Characterizing crustal earthquake slip models for the prediction of strong ground motion, *Seismol. Res. Lett.*, *70*, 59–80.
Süss, M. P., and J. H. Shaw (2003), *P*-wave seismic velocity structure derived from sonic logs and industry reflection data in the Los Angeles basin, California, *J. Geophys. Res.*, *108*(B3), 2170, doi:10.1029/2001JB001628.
Tanioka, Y., and L. Ruff (1997), Source time functions, *Seismol. Res. Lett.*, *68*, 386–400.
Tkalčić, H., D. S. Dreger, G. R. Foulger, and B. R. Julian (2009), The puzzle of the Bardarbunga, Iceland earthquake: No volumetric component in the source mechanism, *Bull. Seismol. Soc. Am.*, *99*, 3077–3085.
Tregoning, P., et al. (1998), Estimation of current plate motions in Papua New Guinea from Global Positioning System observations, *J. Geophys. Res.*, *103*, 12,181–12,203, doi:10.1029/97JB03676.
Tregoning, P., and A. Gorbatov (2004), Evidence for active subduction at the New Guinea Trench, *Geophys. Res. Lett.*, *31*, L13608, doi:10.1029/2004GL020190.
Wallace, L. M., et al. (2004), GPS and seismological constraints on active tectonics and arc-continent collision in Papua New Guinea: Implications for mechanics of microplate rotations in a plate boundary zone, *J. Geophys. Res.*, *109*, B05404, doi:10.1029/2003JB002481.
Zahradnik, J., A. Serpetsidaki, E. Sokos, and G.-A. Tselentis (2005), Iterative deconvolution of regional waveforms and double-event interpretation of the 2003 Lefkada earthquake, Greece, *Bull. Seismol. Soc. Am.*, *95*, 159–172.
Zhao, L., P. Chen, and T. H. Jordan (2006), Strain Green's tensors, reciprocity and their applications to seismic source and structure studies, *Bull. Seismol. Soc. Am.*, *96*, 1753–1763.
Zhao, L., T. H. Jordan, K. B. Olsen, and P. Chen (2005), Fr´echet kernels for imaging regional earth structure based on three-dimensional reference models, *Bull. Seismol. Soc. Am.*, *95*, 2066–2080.
Zhu, L., and X. Zhou (2016), Seismic moment tensor inversion using 3D velocity model and its application to the 2013 Lushan earthquake sequence, *Phys. Chem. Earth*, *95*, 10–18.